

**PARAMETERS EFFECTING THE RHEOLOGY OF PARTICLE FILLED
POLYMERIC SUSPENSIONS**

by

ASLIHAN ÖRÜM

Submitted to the Graduate School of Engineering and Natural Sciences

in partial fulfillment of

the requirements for the degree of

Master of Science

Sabanci University

August, 2013

© Aslıhan ÖRÜM 2013

All Rights Reserved

PARAMETERS EFFECTING THE RHEOLOGY OF PARTICLE FILLED POLYMERIC SUSPENSIONS

Aslıhan ÖRÜM

MAT, Master's Thesis, 2013

Thesis Supervisors: Yusuf Ziya Menciloğlu, Mehmet Yıldız

**Keyword: Agglomeration, Colloidal Suspensions, Fumed Silica, Shear Thickening,
Shear Thinning, Surface Modification**

ABSTRACT

In this work, the rheology of colloidal suspensions composed of low weight fraction, agglomerated, anisotropic particles with flocculated microstructure have studied. Firstly, viscosity and electrical resistance measurements were utilized together with cryo-TEM for conductive particles (CNT and graphene) dispersed in non-conductive media (PEG) so as to address the theoretical gap regarding the shear thickening phenomenon in these suspensions, our results revealed that in the shear thickening region, particles dispersed well due to the instability of the microstructure. Secondly, particles with different morphologies (clay, organoclay, halloysite, CNT, graphene, fumed silica) were also studied to understand the effect of morphology to the rheological behavior of these suspensions. Steady and dynamical rheological measurements were performed to analyze the microstructure formation during flow. Halloysite, clay and organoclay particles and graphene in this research experienced shear thickening behavior under large deformation frequencies; however, suspensions containing CNT showed shear thinning. The results point out that the dispersion of CNTs was hindered due to agglomeration which results in shear thinning behavior. Thirdly, to investigate particle-particle and particle-polymer interactions, the surface of fumed silica particles was modified with silane coupling agents with three different organo-functional groups (epoxy, amine and quaternary ammonium compound). Dynamic light scattering (DLS) results showed that the smaller particle size reflects improved dispersion of modified silica particles in continuous media when compared with that of fumed silica. Shear thickening behavior at earlier critical shear rates (27 s^{-1}) was evidenced by particles covered with epoxy end groups (EPPTMSi); however particles with amine (AEAPTMSi) and quaternary ammonium compound (QuadSi) end functional groups demonstrates shear

thinning behavior. This positive outcome indicates that surface modification of nanoparticles enables designing of "tunable materials" depending on the application with the ease of dispersion. Better dispersion occurs with tunable materials containing easily dispersible nanoparticles. Fourthly, effect of temperature on the rheological response of suspensions was investigated. Temperature sweep results with constant stress showed that gel formation is observed when the temperature reaches to a critical point where sol-gel transition takes place. It is also observed that, the viscosity of all suspensions increase with increasing temperature; because the Brownian motion of silica particles in polymeric media increase with increasing temperature and the hydrodynamic forces induce dilatancy phenomenon. Finally, our results showed that polymeric fluids containing agglomerated, anisotropic particles with low weight fraction (20 wt %) also exhibit shear thickening behavior. This observation differs from relevant research about the rheology of filled polymer systems which are composed of monodispersed, isotropic particles with high volume fraction (40 wt%). Low particle loading provides reduction in weight in terms of shear thickening fluid applications, such as liquid armor, shock absorbent and seismic devices.

PARÇACIK DOLGULU POLİMERİK SÜSPANSİYONLARIN REOLOJİSİNE ETKİ EDEN PARAMETRELER

Aslıhan ÖRÜM

MAT, Yüksek Lisans Tezi, 2013

Tez Danışmanları: Yusuf Ziya Menceloğlu, Mehmet Yıldız

Anahtar Sözcükler: aglomerasyon, kolloidal süspansiyon, füme silika, kayma kalınlaşması, kayma incelmesi, yüzey modifikasyonu

ÖZET

Bu çalışmada, flokule mikroyapıya sahip, düşük konsantrasyonlu anizotropik parçacıklardan oluşan kolloidal süspansiyonların reolojik davranışları incelenmiştir. İlk olarak, belirtilen süspansiyonlardaki kayma kalınlaşması fenomenine ait literatürde yer alan teorik boşluğu ele almak amacıyla, viskozite ölçümleriyle aynı anda gerçekleşen elektriksel direnç ölçümleri ve cryo-TEM analizleri kullanılarak, yalıtkan ortamda (PEG) dağıtılmış iletken parçacıklara (CNT, grafen) ait süspansiyonlar analiz edilmiştir. Elde edilen sonuçlar, kayma kalınlaşması bölgesinde mikroyapıda meydana gelen karasızlık nedeniyle parçacıkların daha iyi dağıldığını göstermektedir. İkinci olarak, morfolojinin bu süspansiyonların reolojisine etkisini incelemek amacıyla, farklı morfolojiye sahip parçacıklar (kil, organo-kil, haloysit, CNT, grafen, füme silika) çalışılmıştır. Akış esnasında mikroyapıda meydana gelen değişimleri incelemek amacıyla, sürekli ve dinamik reolojik analizler kullanılmıştır. Bu çalışmada, kil, haloysit, organo-kil ve grafen yüksek deformasyon frekanslarında kayma kalınlaşması davranışı gösterirken, CNT içeren süspansiyonlar kayma incelmesi davranışı göstermektedirler. Sonuçlar, CNT içerikli dispersiyonlarda aglomerasyona bağlı olarak parçacık dağılımının engellendiğini işaret etmektedir; bu durum kayma incelmesi davranışına neden olmaktadır. Üçüncü olarak parçacık-parçacık ve parçacık-polimer etkileşimini incelemek amacıyla, füme silika parçacıklarının yüzeyi üç farklı organo-fonksiyonel grup (epoxy, amin ve kuaternar amonyum bileşiği) içeren silan ajanları kullanılarak modifiye edilmiştir. Dinamik ışık saçılımı (DLS) sonuçları, modifiye edilen silika parçacıklarının daha küçük parçacık boyutuna sahip olmasından ötürü, füme silikaya göre sürekli faz içerisinde daha iyi dağıldığını göstermektedir. Epoksi sonlu gruplar ile kaplanan silika parçacıklarının (EPPTMSi) daha ileriki kayma oranlarında (27 s^{-1}) kayma kalınlaşması davranışı gösterdiği gözlemlenmiştir. Ancak, amin (AEAPTMSi) ve kuaterner amonyum (QuadSi) sonlu

parçacıklar kayma incelmesi davranışı göstermiştir. Bu pozitif sonuç, daha kolay dispersiyon ile uygulamaya yönelik “ayarlanabilen malzeme” dizaynına işaret etmektedir. Dördüncü olarak, sıcaklığın süspansiyonların reolojisine olan etkisi incelenmiştir. Sabit gerilim altında sıcaklık taraması sonuçlarında; sol-jel dönüşümünün gerçekleştiği sıcaklıkta, jel oluşumunun meydana geldiği gözlemlenmiştir. Ayrıca, sıcaklığa bağlı olarak, silika parçacıklarının polimerik sürekli faz içerisindeki Brownsal hareketinde meydana gelen artış nedeniyle, tüm süspansiyonlarda viskozite artışı gözlemlenmiştir. Hidrodinamik kuvvetler dilatant davranışını tetiklemektedir. Son olarak, sonuçlarımız aglomera halde bulunan, düşük konsantrasyonlu (% 20 k/k) anizotropik parçacık içeren polimerik sıvıların da kayma kalınlaşması davranışı gösterdiğini doğrulamaktadır. Bu gözlem, tek tane boyut dağılımına sahip yüksek konsantrasyonlu (% 40 k/k) izotropik parçacık içeren dolgulu polimerik sistemlerle ilgili reolojik araştırmalardan farklıdır. Düşük parçacık içeriği, sıvı zırh, darbe sönümleyici ve sismik cihazlar gibi kayma kalınlaşması davranışı gösteren sıvıların uygulamalarında, ağırlıkta bir azalma sağlamaktadır.

To my beloved family;
Süheyla, MertCan, and Çetin ÖRÜM

ACKNOWLEDGEMENT

I would like to express my gratitude to all who gave me possibility to complete this thesis. First of all, I would like to thank my advisor, Prof. Dr. Yusuf Ziya Mencilođlu, for his patience, guidance, and support throughout this research. Also, I would like to thank my co-advisor, Assoc. Prof. Dr. Mehmet Yıldız, for his patient guidance, support throughout this research. I am very grateful to work under the supervision of my advisors as a Master student.

I would like to thank Asst. Prof. Dr. Alpay Taralp, Assoc. Prof. Dr. Bahattin Koç and Assoc. Prof. Dr. Melih Papilla for accepting to be my thesis jury.

I would like to acknowledge to Dr. Burçin Yıldız for the Nuclear Magnetic Resonance (NMR) studies as well as her fruitful contributions in NMR analysis during this research. I would like to thank Dr. Burcu Saner Okan for her contributions in Scanning Electron Microscopy analysis and to thank Turgay Gönül for his endless help and sharing of his valuable experiences during my laboratory work. I would like to acknowledge to Prof. Dr. Meriç Özcan for his technical assistance on the electrical resistance measurement experiments in this research.

I would like to thank The Scientific and Technological Research Council of Turkey (TÜBİTAK) for supporting this research as well as providing financial support to my study in Sabancı University. I would like to thank my professors of Materials Sciences and Engineering for their encouragements' and valuable comments and remarks during my study in Sabancı University.

I would like to thank MAT-Grad family for their patience, friendship and support during my time in Sabancı University. Also, I would like to thank my colleagues in FENS 2107 for their help and support. Special thanks to Tuğçe Akkaş, Burcu Saner Okan, Ezgi Dünder Tekkaya, Güliz İnan, Parveen Qureshi and Gönül Kulođlu Kendirici for precious friendship, support and love.

Last but not least, I would like to express my gratitude and give my special thanks to my beloved family for their endless love and support during any era of my life. I can never disregard for their support and unbelievable patience during this research, especially during the times I felt desperate. Special thanks to my parents, Süheyla and Çetin ÖRÜM, for their

precious advice of the life as well as gave me such an amazing brother, Mertcan ÖRÜM. I am very lucky to be the elder sister of him who always makes me smile especially the times I feel miserable and desperate. I can never forget his humor which made me motivated while I was writing this thesis. Many thanks to my mother, who always encourage me and support my decisions and to my father who is also an engineer, and encouraged me to start my engineering career as a Materials Science and Engineer.

TABLE OF CONTENTS

1	INTRODUCTION	1
2	LITERATURE REVIEW	4
2.1	Suspension, Dispersion and Colloids.....	4
2.2	Rheological Behavior of Colloidal Suspensions.....	5
2.3	Viscoelasticity and Measurement	8
2.4	Surface Modification of Silica Nanoparticles.....	10
3	EXPERIMENTAL STUDY.....	13
3.1	Materials	13
3.2	Methods.....	16
3.2.1	Electrical Resistance Measurements.....	16
3.2.2	Surface Modification of Fumed Silica Particles	18
3.2.3	Suspension Preparation.....	19
3.3	Characterization	20
4	RESULTS AND DISCUSSIONS.....	22
4.1	Mechanism behind Shear Thickening Behavior	23
4.2	Particle Morphology Effect.....	27
4.3	Effect of Silica Surface Modification on the Rheology of Colloidal Suspensions..	42
4.3.1	Characterization of Modified Silica Nanoparticles.....	42
4.3.2	Rheological Analysis	47
4.3.2.1	Steady Shear Analysis	47
4.3.2.2	Dynamic Rheological Analysis	52
4.4	Temperature Effect	61
5	CONCLUSION AND FUTURE WORK	63
	REFERENCES	66

LIST OF FIGURES

Fig. 2.1 Flow behaviors of various systems in suspensions [5].....	6
Fig. 2.2. a) Silane coupling agent and functional groups, b) formation of Si-O-Si bonds on substrate surface[30]	11
Fig. 3.1. (a) Aggregate and agglomerate structures [37], (b) SEM micrograph of fumed silica.	13
Fig. 3.2. Custom-made set-up for electrical resistance measurements	17
Fig. 4.1 Comparison of viscosity profile and resistance change in S4 (1 wt% graphene in PEG) suspension under shear forces with time.....	24
Fig. 4.2. Comparison of viscosity profile and resistance change in S1 (1 wt% CNT in PEG) suspension under shear forces with time	25
Fig. 4.3. Comparison of viscosity profile and resistance change in (a) S5 (3 wt% graphene in PEG) and (b) S2 (3 wt% CNT in PEG) under shear forces with time.....	26
Fig. 4.4. (a) cryo-TEM image and (b) resistance measurement with viscosity for S11 (3 wt% graphene in mineral oil)	27
Fig. 4.5. SEM micrographs of (a) halloysite (b) Na-bentonite	28
Fig. 4.6. Viscosity profile of S14 and S15	29
Fig. 4.7. Mechanical spectroscopy of (a) S14 (5 wt% halloysite in PEG) and (b) S15 (5 wt % Na-bentonite in PEG) in LVE.....	30
Fig. 4.8. Mechanical spectroscopy of (a) S14 (5 wt% Halloysite in PEG) and (b) S15 (5 wt% Na-bentonite in PEG) in non-LVE	30
Fig. 4.9. SEM micrograph (scale bar: 1 μ m) for (a) NMT4100 clay and (b) Esan nanoclay..	31
Fig. 4.10. Viscosity profile for S15 (20 wt% NMT4100 clay in PEG) and S16 (20 wt% Nanoclay in PEG)	32
Fig. 4.11. Dynamic rheological analysis for (a) S19 (20 wt% Nanoclay in PEG) and (b) S17 (20 wt% NMT4100 clay in PEG) in LVE	33
Fig. 4.12. Strain sweep results for (a) S19 (20 wt% Nanoclay in PEG) and (b) S17 (20 wt% NMT4100 clay in PEG) with varying deformations frequencies.	34

Fig. 4.13. Dynamic rheological result of (a) S19 (20 wt% Nanoclay in PEG) and (b) S17 (20 wt% Nanoclay in PEG) (under 0.1 strain)	35
Fig. 4.14. Viscosity profile of S15 (5 wt% Na-Bentonite in PEG), S16 (5 wt% NMT4100 clay in PEG) and S18 (5 wt% nanoclay in PEG)	36
Fig. 4.15. Dynamic rheological result of (a) S16 (5wt% NMT4100 clay in PEG) and (b) S18 (5wt% nanoclay in PEG)	37
Fig. 4.16. SEM micrograph (scale bar: 2 μ m) for CNT that was used in this study	37
Fig. 4.17. Viscosity profile for (a) S3 (5 wt% CNT in PEG) and (b) S13 (10 wt% CNT in PEG) at 5k and 10 kPa max. shear stresses	38
Fig. 4.18. cryo-TEM images (scale bar: 200 nm) for CNT filled PEG suspensions; (a) S3 and (b) S13.....	39
Fig. 4.19. Frequency sweep analysis of (a) S3 (5 wt% CNT in PEG) and (b) S13 (10 wt% in PEG) in LVE region.....	39
Fig. 4.20. (a) and (b) SEM images (scale bar: 1 μ m) of graphene.	40
Fig. 4.21. Viscosity profile at (a) 100 and (b) 5000 max. shear stresses, (c) and (d) cryo-TEM images (scale bar: 1 μ m) of S6 (5w% graphene in PEG)	41
Fig. 4.22. Frequency sweep analysis of S6 (5 wt% in PEG) in LVE	42
Fig. 4.23. FT-IR spectra for HFSi, EPPTMSi, AEAPTMSi, QuadSi.....	43
Fig. 4.24. Comparative ¹ H-NMR spectra of silane coupling agents, fumed silica and modified silica particles respectively (a) EPPTMS-HFSi-EPPTMSi (b) AEAPTMS-HFSi-AEAPTMSi (c) Quad silane (quaternary ammonium compound)-HFSi-QuadSi	44
Fig. 4.25. TGA results of HFSi, EPPTMSi, AEAPTMSi, and QuadSi.....	45
Fig. 4.26. TEM images of silica particles before and after modification: (a) HFSi	47
Fig. 4.27. Viscosity curves for unmodified and modified silica particles in (a) PEG and (b) PPG	48
Fig. 4.28. cryo-TEM images (scale bar: 100 nm) for (a) C1 (b) C2 (c) C3 (d) C4 (e) C5 (f) C6 (g) C7 (h) C8.....	51
Fig. 4.29. DLS results of C1 (20 wt% HFSi in PEG) and C5 (20 wt% HFSi in PPG).....	51
Fig. 4.30. Dynamic oscillatory frequency sweep in LVE region for suspensions;.....	54

Fig. 4.31. Elastic and viscous modulus of colloids at varying frequencies; 10, 20, 50 and 100 rad/s.....	56
Fig. 4.32. Frequency sweep analysis in non-LVE region for (a) C1 (b) C2 (c) C3 (d) C4 (e) C5 (f) C6 (g) C7 (h) C8.....	59
Fig. 4.33. Single frequency experiments results for samples C1-C8: (a) Elastic modulus (b) Viscous modulus.....	60
Fig. 4.34. Viscosity profile of colloidal suspensions with temperature change (25-125°C) ...	62
Fig. 4.35. Dynamic rheological response of (a) C1 and (b) C3 within the temperature range of 25-125°C.....	62

LIST OF TABLES

Table 1. Chemical properties of silane agents	15
Table 2. Properties of continuous media used in experimental study.....	16
Table 3. Compositions of suspensions.....	19
Table 4. Summary for flow behavior and hydrodynamic radius of suspensions C1-C8.....	52

LIST OF ABBREVIATIONS

- AEAPTMS: 3-[2-(2-Aminoethylamino)ethyl-amino]propyl-trimetoxy-silan
- AEAPTMSi: 3-[2-(2-Aminoethylamino)ethyl-amino]propyl-trimetoxy-silan modified silica
- QuadSi: silica particles modified with quaternary ammonium compound
- CNT: Carbon Nanotube
- DLS: Dynamic Light Scattering
- EPPTMS: [3-2,3-Epoxy-propoxy-propyl]-trimetoxy-silan
- EPPTMSi: [3-2,3-Epoxy-propoxy-propyl]-trimetoxy-silan modified silica
- HFSi: Hydrophilic Fumed Silica
- FT-IR: Fourier Transform Infrared
- NMR: Nuclear Magnetic Resonance
- LAOS: Large Amplitude Oscillatory Shear
- LVE: Linear viscoelastic
- PDI: Poly Dispersity Index
- ODT: Order to Disorder Transition
- PEG: Polyethylene glycol
- PPG: Polypropylene glycol
- SAOS: Small Amplitude Oscillatory Shear
- SEM: Scanning Electron Microscopy
- TGA: Thermo Gravimetric Analysis
- TEM: Transmission Electron Microscopy

CHAPTER I

1 INTRODUCTION

Particle filled polymeric fluids have a wide range of applications in the industry, especially ceramic, paint, food, cosmetics, pharmaceuticals, and so on. The dispersion of these fluids show Non-Newtonian behavior during flow and processing: shear thinning is the decrease of viscosity with increasing shear stress; the contrary behavior, shear thickening is the increase of viscosity with increasing shear stress. The later behavior is undesirable in the processing industry because it damages the processing equipment during flow. However, this undesirable behavior has received great interest in recent years in the engineering applications. Much research has been conducted on the application of shear thickening fluids. These energy absorbance applications can be listed as: liquid armor in defense; shock absorbing devices such as suspension systems or dampers in automobiles; seismic protectors for buildings; as well as biomedical and sport devices [1, 2, 3]

There has also been significant research devoted to understanding the origin of the shear thickening phenomenon. Two accepted explanations of this phenomenon have emerged: Order to Disorder Transition (ODT) and Hydrodynamic Clustering Theories. The former proposes that monodispersed particles are hexagonally packed within the fluid layers in concentrated dispersions. Repulsive forces at low shear rates are responsible for shear thickening [1, 2]. The second theory; Hydrodynamic Clustering, suggests that hydrodynamic forces in concentrated hard sphere systems (i.e. 40wt%) cause the percolation of repulsively interacting particles [3]. However, these well known theories do not explain the shear thickening phenomenon in suspensions filled with low concentration, agglomerated, anisotropic particles.

Apart from these two phenomena of flow behavior, many other parameters control the rheology of these suspensions. Genovese et.al, summarize these parameters such as particle size, particle structure and morphology, particle concentration, particle-particle and particle-polymer interactions [4]. It was reported that anisotropy in particles

changes the rheological behavior from shear thinning to shear thickening. According to net attractive forces between particles, two possible structure formations are observed in colloidal dispersions. If the interaction is weak, weakly aggregated structures are formed in a colloid. This formation is called flocculation and is reversible. However, strong particle-particle interaction can lead to form a coagulation that is irreversible. such strong gels are observed when network formation is confined [4].

To date much research has been focused upon shear thickening behavior of suspensions containing monodispersed, isotropic particles with high volume fraction. Little work, on the other hand, has been done on shear thickening behavior of suspensions containing agglomerated, anisotropic particles with low volume fraction. The purpose of this study is thus to complete this gap in the literature as well as investigating the parameters affecting the rheological behavior of polymeric fluids containing nanoparticles. Four areas were under concern: Mechanism behind the shear thickening phenomenon in suspensions filled with agglomerated particles, effect of particle morphology on the shear thickening behavior, effects of silica particles surface modification on the rheology and lastly effect of temperature on the viscosity and microstructural development of suspensions containing modified silica particles.

In this regard, suspensions composed of anisotropic, agglomerated particles with low weight fraction (20 wt% and < 20 wt%) have been studied to shed light upon the mechanism of shear thickening behavior of particle filled polymers. To address a theory for particle filled polymers, electrical resistance measurements were then utilized with viscosity measurements. Diverse particles with different morphologies were studied to investigate the effect of particle structure. Steady and dynamic rheological measurements were done to understand the microstructure development under low and high shear stresses. Silica particles were also modified to understand the effect of the particle-polymer and particle-particle interactions. After ensuring the success of chemical modification with several relevant characterization methods (¹H-NMR, FT-IR, and TGA), steady and oscillatory shear experiments were performed to reveal the dominant forces on colloidal suspensions. High shear and low shear forces determined the choice as to small amplitude oscillatory shear (SAOS) and large amplitude oscillatory shear (LAOS) experiments. Because of LAOS experiment's tendency to disturb the microstructure, we employed it to monitor microstructural development

under high shear; SAOS, on the other hand, was then used to reveal the microstructure at equilibrium states. Lastly, to investigate the effect of temperature on the flow and deformation behavior of suspensions, temperature sweep experiments in range from 25°C to 125°C were performed. Suspensions containing silica and modified silica particles were performed. From our results, we propose that shear thickening behavior takes place due to rearrangement of particles with applied forces; the large amount of shear forces break down the order structure into a disordered state. Strong particle-particle interaction leads to form agglomerated structure that then results in network structure. This network formation hinders better dispersion; thus, reversing the behavior of shear thickening.

CHAPTER II

2 LITERATURE REVIEW

2.1 Suspension, Dispersion and Colloids

Suspension is a generic term for a biphasic system in which both discrete phase (solid particles) and continuous phase (liquid or fluid) exist in the same volume. Dispersion, on the other hand, is the particular case of a dispersed suspension, in which particles should be kept apart from each other due to the action of either shear forces or repulsive (or dispersive) interparticle forces. [4, 5]. The term “Colloid” generally refers to a biphasic system in which the elements of discrete phase are too small to be observed by microscopy [6]; in other words, the size of particles in the discrete phase are in a colloidal range which varies from 1nm to 1 μ m[6]. According to dominant forces acting on the discrete phase, suspensions can be divided into three groups:

- a) **Hard-sphere suspensions:** discrete phase is composed of rigid, spherical and inert particles are called as hard spheres; there is no interparticle forces
- b) **Dispersed or stabilized suspensions (dispersions):** a net repulsive force between particles keep them separated
- c) **Aggregated suspensions:** net attractive forces are dominant and causes flocculation and aggregation. When the aggregates interconnect into a network above gelation concentration, they form a gel. Regarding the degree of agglomeration, these gels are classified as:
 - i. **Weakly aggregated suspensions:** these are weak gels in which the aggregation is not strong and reversible. This reversible process is called “flocculation”
 - ii. **Strongly aggregated suspensions:** these suspensions are colloidal gels where strong and irreversible aggregation, which is called coagulation, occurs [4].

Hydrodynamic, Brownian, and colloidal forces coexist in various degrees in suspensions that flow. The first one, hydrodynamic or viscous forces which arise from the relative motion of particles to the surrounding fluid, are in all flowing suspensions. The second one, identified as Brownian forces, are thermal randomizing forces which always exist in the system. The last one, colloidal forces, are potential forces which can be described as elastic.[4]. The degree of existence and/or dominance arising from these forces is affected mainly by the particle size of the discrete phase in the flowing suspension. For suspensions with a particle size larger than $\sim 10 \mu\text{m}$, hydrodynamic forces are dominant; however, for colloidal suspensions, Brownian, hydrodynamic and interparticle forces are equally dominant in the flow of colloids. The rheology of colloidal suspensions depends on the particle size, the shear rate, as well as the characteristics of continuous phase (e.g. viscosity) and of discrete phase such as interparticle interactions (e.g. Van der Waals interactions, electrostatic and steric repulsions). According to dominant forces acting on and effective interactions in the system, colloidal suspensions exhibit complex non-Newtonian flow behavior (either shear thinning or shear thickening) when they are subjected to external forces.

2.2 Rheological Behavior of Colloidal Suspensions

As mentioned in section 2.1, colloidal suspensions show a deviation from linearity (Newtonian) in their flow behavior; that is to say, they do not obey Newton's law:

$$\eta = \frac{\tau}{\dot{\gamma}}$$

τ is the shear stress, η is the viscosity, and $\dot{\gamma}$ is the shear rate. They show a

change in their viscosity with applied shear. Various flow behaviors (Fig.2.1) are observed in colloidal suspensions; among these non-Newtonian flow types, pseudoplastic that is also identified as “shear thinning behavior” and dilatant that is also identified as “shear thickening behavior” are most commonly seen in colloidal suspensions.

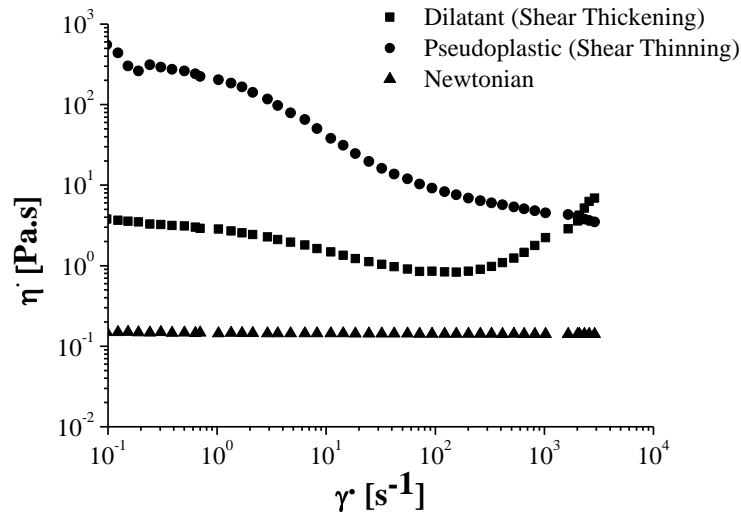


Fig. 2.1 Flow behaviors of various systems in suspensions [5]

“*Shear thinning behavior*” is distinguished by the gradual decrease in the viscosity with increasing shear rate. Shear thinning is a time-independent flow behavior [7]; the viscosity is dependent only the value of applied shear stress or shear rate, not dependent on the time of the applied force [8]. Shear thinning behavior is commonly found in blood, paint and ceramic slurries. Another example of shear thinning behavior, widely used in Li battery technology, is the mixture of polymer electrolyte and small size inorganic particles [9, 10]. Agglomeration induces shear thinning behavior in suspensions; increased shear rate will break down the agglomerates, as a result, amount of immobilized continuous phase due to the aggregated particles will be reduced and then the viscosity of the suspension will decrease [7]. Shear thinning is also a familiar phenomenon in polymer solutions and molten polymers. This flow type aids the transport of these type of fluids through processing equipment because the pressure drop at the walls is reduced due to the decrease in the fluid viscosity [11].

“*Shear thickening behavior*” is identified by the increase in the viscosity with applied shear forces [7] and as shear thinning, shear thickening is also time-independent Non-Newtonian flow [8]. Common examples of shear thickening behavior in suspensions are cornstarch dispersed in water or milk, as well as wet sand and some polyvinyl in chloride sols [9,8]. It is a fully reversible process; meaning that, as soon as the shear rate is decreased, the viscosity will decrease immediately no matter whether or not the viscosity is high [9]. Concentrated suspensions of hard spheres exhibit shear thickening

behavior; these Brownian hard spheres induce the hydrodynamic forces at high shear rates [9]. The mechanism behind the shear thickening phenomenon in concentrated suspensions will be explained simply in the following paragraph below. However, as Barnes reported in his seminal review all suspensions show shear thickening under right circumstances [2]. Contrary to the shear thinning, the shear thickening phenomenon is not a preferred fluid behavior in certain industrial processes [2] such as polymeric nanocomposites manufacturing process since it adversely affects the performance of the process as well as the process-ability of material and prevents proper materials handling [9]. The shear rate and also the viscosity of shear thickening fluid are at the maximum level at the walls of the processing equipment. This causes pressure built-up. However, the shear thickening behavior of colloidal suspensions can be advantageous for some other specific applications and thus, have resulted in a tremendous amount of industrial and commercial innovations in many areas. For example, shear-thickening fluids can be used for applications such as liquid armor in defense; shock absorbing devices such as suspension systems or dampers in automobiles; seismic protectors for buildings, biomedical and sport devices, among others [12-18].

There has been significant research devoted to understand the origin of the shear thickening phenomenon. Two accepted theories explain the mechanism behind this phenomenon. These are Order to Disorder Transition (ODT) and Hydrodynamic Clustering. The first theory proposes that monodispersed particles are hexagonally packed within the fluid layers in concentrated dispersions. This happens due to the repulsive forces at low shear rates. At higher shear rates, however, the magnitude of shear force becomes larger than interparticle forces. As a result, the order in the particle configuration gets disrupted, thereby causing an increase in particle interactions. This results in a rise in the viscosity of the suspension at a critical shear rate [1, 19]. The Hydrodynamic Clustering theory on the other hand suggests that hydrodynamic forces in concentrated hard sphere systems (i.e. 40 wt%) cause the percolation of repulsively interacting particles [3, 20]. These two well known theories are advocated relying on the results of the light/neutron scattering experiments as well as Stokesian Dynamic simulations [21] for the suspensions of sterically or electrostatically stabilized monodispersed spheres. Since these two theories can explain the shear thickening mechanism in colloidal systems with high volume fraction and non-flocculated particles (formed due to the electrostatic and steric repulsive interactions), they do have

difficulties in addressing shear thickening behavior in suspensions with low volume fraction and flocculated particles [2]. In their work, Negi et.al and Osuji et.al reported that shear thickening exists in attractively interacting colloidal suspensions. They attributed the shear thickening phenomenon to the breaking down of dense fractal clusters and associated with a increase in the effective volume fraction of particles in the colloids [22, 23]. Although a large body of study has been published on the rheology of colloidal suspensions, given the fact that many different types of colloidal systems can be formed, it can be quite challenging to develop a single theory capable of addressing all aspects of the shear thickening mechanism for every suspension. Consequently, the driving forces behind the shear thickening behavior of complex fluids have not been fully understood yet and have remained an ongoing controversial issue in the relevant literature.

2.3 Viscoelasticity and Measurement

Many materials can be readily classified as solids or fluids, displaying elastic and viscous behavior, respectively. However when a material possess the combination of these two behaviors, then this material is named as viscoelastic [24] The term ‘viscoelasticity’ implies that the substance under consideration has both viscous and elastic properties; in other words combines properties of elastic solid and viscous fluid [6, 25]. When a material exhibits perfect elastic behavior, the elastic solid possesses perfect memory for its non-deformed state; as the applied deformation is removed, the body turns to an initial non-deformed state immediately. A fluid, on the other hand, possesses no memory regarding to the non-deformed state, so the fluid will still remain in its deformed state. The deformation is time-independent in an elastic solid; however, in a viscous fluid, the deformation is time-dependent. Lastly, in the energetic view, the work done in an elastic deformation is stored as potential energy and it is recovered never the less, in the viscous flow, energy dissipation happens and the loss of the energy is not recovered [6].

Oscillatory shear is widely used in characterization of viscoelastic materials. The measurement procedure is the same with the steady shear measurements where the

viscosity curve is obtained (The material behavior, as apprehended by steady viscosity, is not dependent on the direction of rotation; $\eta = \eta(\dot{\gamma}) = \eta(-\dot{\gamma})$). The difference in oscillatory shear method is that stress and strain vary sinusoidally and they are recorded as a function of time. Relative contributions of viscous and elastic responses of the material at different frequencies can be measured with this method; thus, this method is also referred to as mechanical spectroscopy [25]. The stress-strain relation in that method is given by the formula; $\sigma = \gamma[G'(\omega) \sin(\omega t) + G''(\omega) \cos(\omega t)]$ where $\sigma, \gamma, \omega, G', G''$ are the stress, the strain amplitude, the frequency, elastic modulus, and viscous modulus, respectively. The stress component in-phase with the deformation defines the *elastic* (or storage) modulus G' which is related to the elastic energy stored in the system on deformation whereas the stress component out-of-phase with the strain gives the *viscous* (or loss) modulus G'' which is linked to the viscous dissipation of the energy in a system [26].

When oscillatory shear is used as a mechanical spectroscopy to monitor the microstructure of a complex fluid under different conditions, two classes of oscillatory shear are applied in viscoelastic measurements. Small amplitude oscillatory shear (SAOS) is applied to monitor microstructure in the material at low deformations as well as observance of the equilibrium state microstructure whereas the large amplitude oscillatory shear (LAOS) is applied to highlight the structural changes taking place in the material at large deformations[25]. SAOS represents the *linear viscoelastic response* of the material; the relation between stress and deformation of a material near equilibrium usually occurs when the deformation is small. In SAOS G' and G'' are not functions of strain amplitude; stress-strain relation in linear response of the material is reduced to $\sigma = G'(\omega) \sin \omega t + G''(\omega) \cos \omega t$. However, in LAOS, nonlinear responses such as structural changes and phase transitions are monitored. Linear response is usually very important to understand the basic mechanisms responsible for material behavior. Nonlinear response, on the other hand, is more relevant for applications [25].

2.4 Surface Modification of Silica Nanoparticles

Nanoparticles are widely used in many industrial applications to improve the performance of materials in terms of mechanical, electrical, thermal properties.. Since the nanoparticles have positive outcomes regarding material properties, dispersion of the nanoparticles is still a controversial issue in processing industry. Much research has been devoted to improve the dispersion of nanoparticles.

Among nanoparticles, silica is widely used in polymers to improve their scratch resistance and mechanical properties. The surface of silica particles is natively composed of siloxane and silanol groups. The latter are prone to form hydrogen bonds either with solvent, residual water, or other silanol groups of closely spaced silica nanoparticles [27]. These silanol groups make the surface of silica particles hydrophilic. Although these silanol groups are very weak acids and are hardly reactive, it is still possible to chemically convert them so that the interaction between polymer and particles can be tuned upon application[27, 28]. There are basically two methods to modify silica particles: physical interaction and chemical interaction [29]. Surface modification through physical interaction is generally accomplished with the use of surfactants or macromolecules adsorbed onto the surface of silica particles. The preferential adsorption of a polar group of a surfactant to the surface of silica is accomplished by electrostatic interaction. This process is the principle of surfactant treatment. A surfactant is able to decrease the formation of agglomerate within the silica particles by diminishing physical interaction; thus particles can incorporate into polymer matrix [29]. In chemical interaction; modification is achieved by either modification agents or by grafting polymers. Silane coupling agents are the most used type of modifier agents. They generally have hydrolysable and organofunctional ends [29]. Most widely used silane coupling agents are chlorosilanes, alkoxysilanes, silazanes and siloxanes. In most cases, modification ensures modified pyrogenic silicon dioxides to exhibit hydrophobic surfaces [28]. Surface modification via chemical interaction is much more favorable than physical interaction since surface modification can lead to much stronger interaction between modifiers and silica nanoparticles [29].

The pathway during modification of silica particles via chemical interaction is depicted in Figure 2.1: a) Silane coupling agent and functional groups, b) formation of Si-O-Si bonds on substrate surface [30].

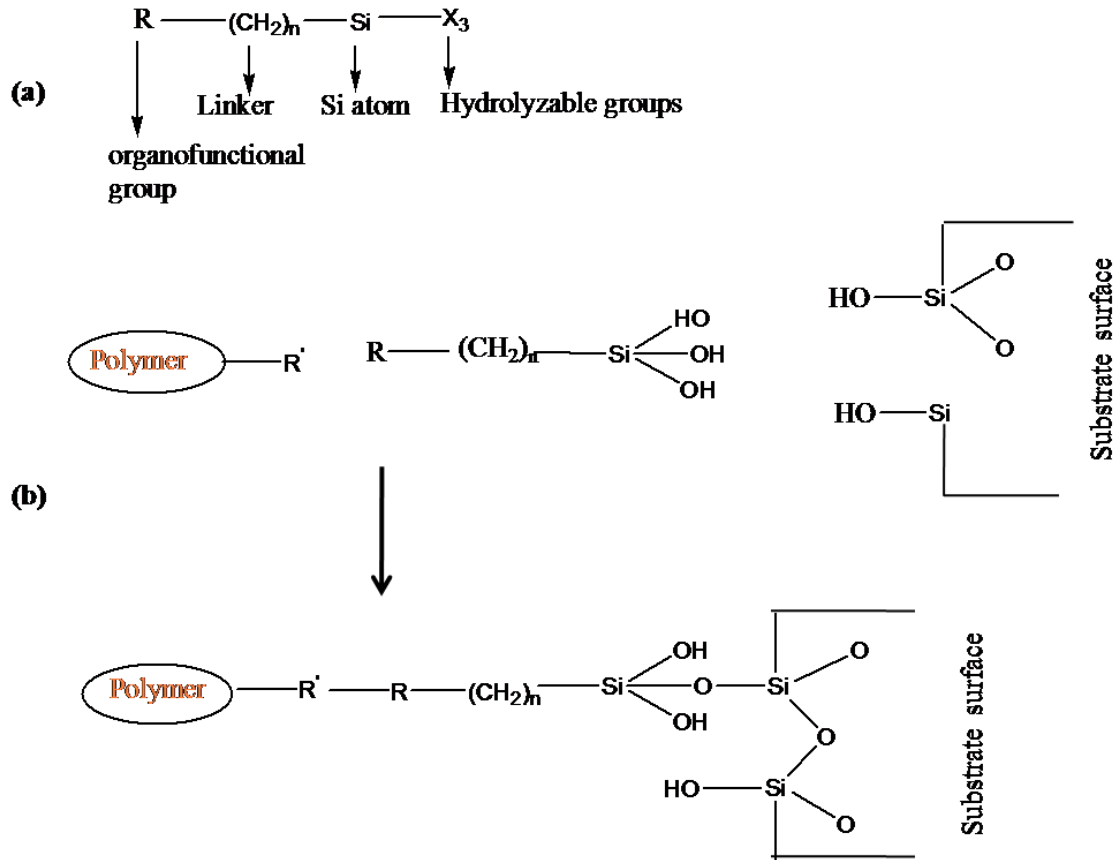


Fig. 2.2. a) Silane coupling agent and functional groups, b) formation of Si-O-Si bonds on substrate surface[30]

A vast amount of research has been done the modification of nanoparticles [31, 32] as well as fumed silica, regarding tuning the surface properties [29, 30, 33-35]. Among them, there is little detailed research about rheological behaviors modified silica particle in polymers and about performance of these tunable materials in shear thickening fluid applications.

Mahfuz et.al report in his work that surface modified silica particles provides enhanced stab resistance to Kevlar when impregnated with STF (shear thickening fluid). Functionalization of silica particles enhances bonding with silica and PEG. This improves the composite performance significantly in terms of energy absorbance [30]. However, Francisco et.al show non-flocculated suspension formation in polypropylene glycol with silica particles modified with alkyl groups, these alkyl groups make the surface hydrophilic and since modified particles are formed into a gel in a polar organic

solvent, shear thinning behavior was observed in the suspension [31]. Cao et.al report that surface treatment of silica particles with ethylene glycol by chemical methods provides a high amount of particle loading since surface treatment hinders agglomeration of silica particles and enhances their dispersion. However, no significant change was reported in terms of shear thickening response of the colloidal suspensions since the network formation still sustained. However, surface treatment provided the increase of weight fraction thus, improving shear thickening behavior due to ease of cluster formation [35]. These findings show that; surface modification ensures tunable materials production in terms of surface properties and desired particle-polymer interaction.

CHAPTER III

3 EXPERIMENTAL STUDY

3.1 Materials

The structure, chemical and physical properties of the materials used in this study are given in detail below. In the suspensions, fumed silica, clay, nanoclay, halloysite, CNT and graphene were used as the particles and polyethylene glycol, polypropylene glycol and mineral oil were chosen as continuous media. [3-2,3-Epoxy-propoxy-propyl]-trimethoxysilane, 3-[2-(2-Aminoethylamino)ethyl-amino]propyl-trimethoxysilane, and quaternary ammonium compound were used as silane coupling agents for surface modification.

Fumed silica is a synthetic, and amorphous form of silicon dioxide (SiO_2) produced via flame hydrolysis of silicon tetrachloride (SiCl_4) with H_2 and O_2 . The exposure of primary silica particles to high temperature during the production stage converts its structure into the form of an aggregate which contains the unique properties of this particular type of silica particles. Therefore, primary flow units in suspensions are aggregates, not individual particles of silica. The BET surface area of particles is 100-140 (m^2/g) and the silanol group (Si-OH) density is 2 SiOH/nm^2 [36].

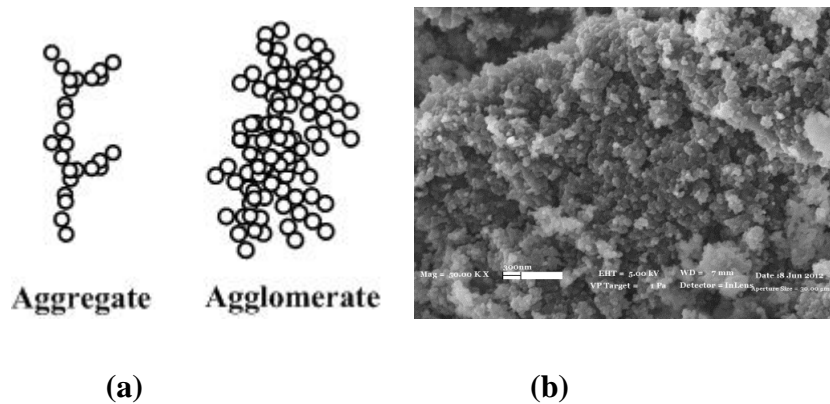


Fig. 3.1. (a) Aggregate and agglomerate structures [37], (b) SEM micrograph of fumed silica.

Two types of graphitic base carbon material were used in this study. These are multiwall carbon nanotube (CNT) purchased from Bayer GmbH (BAYTUBES) and graphene which was synthesized regarding the technique used by Saner et al [38].

CNTs consist of graphene sheets rolled into tubes. The diameters of the tubes are of the order of 1–100 nm and the lengths are usually up to the 1 m range. They have large aspect ratios. They have high affinity to agglomerate due to their electronic structure. They have high mechanical properties, high thermal and electrical conductivity with low density. In this study, multiwalled carbon nanotubes (MWCNT) were used which consist of multiple concentric graphene cylinders and are the most commercially available form of CNT [39, 40].

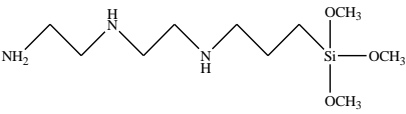
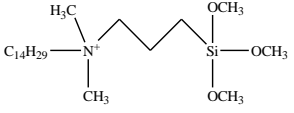
Graphene is a material composed of pure carbon, with atoms arranged in a regular hexagonal pattern. Graphene is the basic structural element of some carbon allotropes including graphite, charcoal, carbon nanotubes and fullerenes. It can be described as a one-atom thick layer of mineral graphite. When many layers of graphene are stacked together, they effectively form crystalline flake graphite. Graphene is very light, with a 1-square-meter sheet weighing only 0.77 milligrams. As the source of CNT, graphene has properties similar to those of CNT [41, 42].

Four different silicate based materials were used to study the particle morphology effect on rheology. These are purified clay (Na-Bentonite, Esan Inc.) two different types of commercial organo-clay and halloysite (Esan Inc.). Organoclays are sodium clay from Reşadiye region (NMT4100 clay, NanoInvent Inc.) that is modified with quaternary ammonium compound and nano clay (Esan Inc.) which is also modified with quaternary ammonium compound after purification.

Layered silicates crystal lattice consists of two-dimensional layers. Two external silica tetrahedron are fused with central octahedral sheet of alumina or magnesia by the tip so that the oxygen ions of the octahedral sheet do also belong to the tetrahedral sheets. These layers organize themselves to form stacks alternated by a regular van der Waals gap. These gaps are identified as the interlayer or the gallery. Isomorphic substitution within the layers (for example, Al_3) is replaced by Mg_2 , or by Fe_2 , or Mg_2 replaced by Li. This substitution generates negative charges. They are counter balanced by alkali or alkaline earth cations situated in the interlayer. The forces that hold the stacks together are relatively weak; thus, intercalation of small molecules between the layers is easy to perform [43].

In order to observe the effect of surface modification of fumed silica particles on the shear thickening behavior of the colloidal system, particles were modified with organofunctional alkoxy silanes with different polarities. To do so, amine and epoxy based silane coupling agents (Gelest Inc.) and partially quaternized organosilane composition under the trade name “Antimic6000™” (Nanotego Inc) were chosen. Chemical properties of these silanes are given in Table 1. Commercial hydrophilic fumed silica particles (HDK N20) (Wacker Chemie A.G) are selected as starting material.

Table 1. Chemical properties of silane agents

Silane agents	Chemical structure	Density (g/ml)
[3-2,3-Epoxy-propoxy-propyl]-trimethoxysilane (EPPTMS)		1,07
3-[2-(2-Aminoethylamino)ethyl-amino]propyl-trimethoxysilane (AEAPTS)		0,857
Quaternary Ammonium Compound (Antimic6000)		1,024

Two types of polymeric fluids, PEG (Merck Inc.) and PPG (Dow Chemicals Inc.) with a molecular weight of 300 g/mol (Table 2) were chosen as continuous media to disperse modified and non-modified silica particles to understand particle-matrix interaction in suspensions. For electrical resistance measurement, PEG and mineral oil (Fluka) were used to disperse conductive particles (CNT and graphene) in a non-conductive medium. Mineral oil was chosen over polyethylene glycol to achieve better dispersion of conductive particles. Since the particles and continuous media are both non-polar molecules, they do not possess net dipole moment due to their symmetrical structure. Thus, the conductive particles can disperse in mineral oil well compared to in polyethylene glycol.

Polyethylene glycol (PEG) is an oligomer of ethylene oxide with a linear chain structure. It has two –OH groups on its linear chain. These hydroxyl groups give polymer a polar structure. Polypropylene glycol (PPG) is an oligomer of propylene glycol with a linear chain structure. PPG has also hydroxyl end groups like PEG; however, -CH₃ in linear chain makes the polymer less polar compared with the polarity of PEG.

Mineral oil is a light mixture of alkenes in C₁₅ and C₄₀ range. It is a liquid by-product of the distillation of petroleum. It is primarily composed of alkenes and cyclic paraffins which makes the structure non-polar.

The structural, chemical and physical properties of continuous media are given in Table 2.

Table 2. Properties of continuous media used in experimental study

Continuous media	Molecular weight (g/mol)	Molecular structure	Viscosity (η) (Pa.s)	Density (ρ) (g/ml)
Polyethylene glycol (PEG)	200	OH-CH ₂ -(CH ₂ -O-CH ₂) _n -CH ₂ -OH	0.056	1.125
Polyethylene glycol (PEG)	300	OH-CH ₂ -(CH ₂ -O-CH ₂) _n -CH ₂ -OH	0.077	1.125
Polypropylene glycol (PPG)	300	H-(O-CH-(CH ₃)-CH ₂) _n -OH	0.280	1.080
Mineral oil	310	CH ₃ -(CH ₂) ₂₀ -CH ₃	0,025	0.850

3.2 Methods

3.2.1 Electrical Resistance Measurements

Electrical resistance measurements performed simultaneously with rheological measurements was been conducted in order to reveal the microstructural change of

colloidal suspensions in shear thinning and shear thickening region. In this regard, carbon nanotubes (BAYTUBES) and graphene that are both conductive were dispersed in polyethylene glycol (Merck Inc.) which is a non-conductive media. A custom-made system was used (Fig.3.2) to monitor the microstructural change in rheological properties of colloidal dispersions. A digital multimeter (Agilent 34410) was connected to the rotational rheometer (Gemini II, Bohlin) in order to monitor the electrical resistance change of these suspensions under shear. LabVIEW code was used to transfer the data during the experiment.

Electrical resistance measurements were performed on the 2-wire resistance principle. In this principle, the resistance of the sample that is placed between two copper wires is measured under low voltage (According to Ohm Law; $V = I.R$ and then resistance (R) can be measured with applied voltage (V)). The input and output that come from the multimeter are connected with a cable to electro-rheology (ER) cell and to the probe. These input and output cables are placed between the stainless steel disk and the stainless steel parallel plate, respectively. The input connection (Fig.3.2.b) applies a low amount of voltage to the sample; the output (Fig.3.2.b) provides the electrical resistance change in the sample to which shear force is applied.

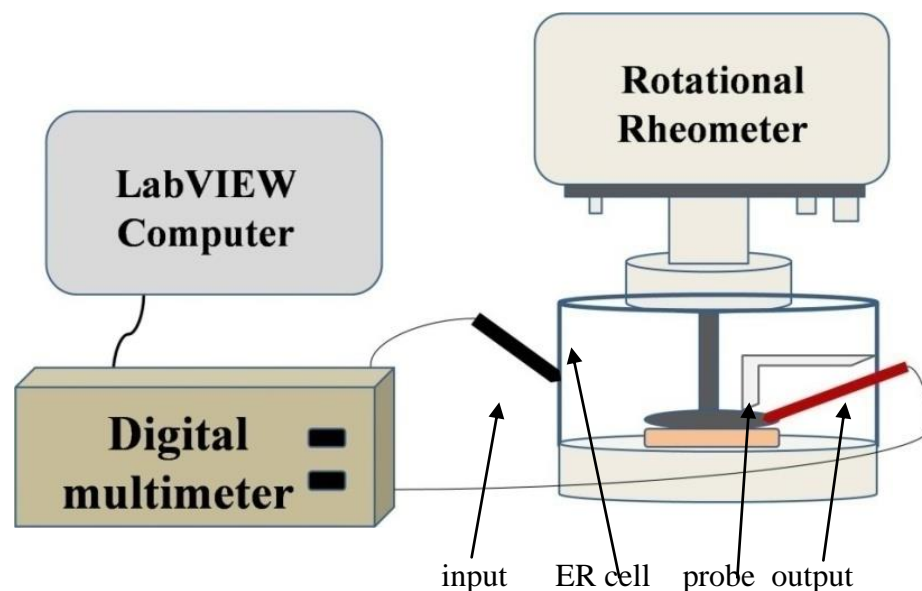


Fig. 3.2. Custom-made set-up for electrical resistance measurements

$R = \frac{\rho \cdot l}{A}$; where ρ is the specific resistance of the material, l is the length of the material (here, gap size) and A is the area (here, the area of the parallel plate that is used in the measurements). σ , conductivity, $\sigma = \frac{1}{\rho}$ has a relation with resistance given in that equation; it also changes with temperature. For that reason, temperature is another control parameter for the resistance measurements under stationary conditions. Because of the ascendant parameters such as A , l , *temperature and time* which affect the resistance, designating the correct parameters in resistance measurements is important. Gap size (l) and diameter of the plate (A) are also crucial for the rheological measurements. To sum up, reliability tests have been performed to determine the correct gap size and correct parallel plate diameter. After determination of gap size and plate diameter, reliable and reproducible results were obtained during experiments for resistance measurements. All measurements for electrical resistance characterization during stationary and steady shear conditions were repeated three times.

Suspensions with 3 different weight percentages (1%, 3%, 5%) of particles were prepared by using a high shear mixer with a speed of 5000 rpm for 30 minutes. Electrical resistance and viscosity profile results for these suspensions are given in *Section 4.1*

3.2.2 Surface Modification of Fumed Silica Particles

Modification of fumed silica particles with different silane coupling agents were done as follows: Particles were dispersed into an ethanol (Merck Inc.) environment by using an ultrasonic bath until obtaining low hydrodynamic radius and polydispersity index (PDI) value. Hydrodynamic radius and PDI values were measured and confirmed by DLS (Malvern Zeta Nanosizer). Organo-silane compounds were added to the mixture as 5% wt of silica particles. Due to the quaternary ammonium compound's long alkyl chain which inhibits an effective surface interaction with particles, it comprised 10% wt of the silica particles. After a 60 hour reaction in ethanol environment, the hydrodynamic radius of particles in that media were measured. Then, modified silica particles were centrifuged at 4900 rpm for 5 hours to decrease the amount of loss of silica particles in supernatant and thoroughly washed with ethanol for four times in

order to remove the non-reacting organosilane compounds. Particles were dried in a vacuum oven overnight at 120°C to remove volatiles.

3.2.3 Suspension Preparation

All suspensions were prepared by using a shear mixer with a rotation of 5000 rpm until a homogenous colloidal system was obtained. Suspensions were prepared as wt/wt basis (particle/polymer). They are labeled as “C” for colloid and “S” for suspension. They are coded based on particle size in a suspending medium whether they are in a colloidal range or not. Composition and particle concentration of the suspensions are given in Table3. Silica particles after surface modification are labeled as follows: EPPTMSi for particles modified with epoxy end silane agent, AEAPTMSi for particles modified with amine end silane agent, and QuadSi for particles modified with quaternary ammonium compound.

Table 3. Compositions of suspensions

			Continuous Phase			
			PEG200	Mineral oil	PEG300	PPG300
Discrete Phase		wt%				
	CNT	1	S1	S7		
		3	S2	S8		
		5	S3	S9		
		10	S13			
	Graphene	1	S4	S10		
		3	S5	S11		
		5	S6	S12		
	Halloysite	5	S14			
	Na-Bentonite	5	S15			
	NMT4100 clay	5	S16			
		20	S17			
	Nanoclay	5	S18			
		20	S19			
	HFSi	20			C1	C5
	EPPTMSi	20			C2	C6
AEAPTMSi	20			C3	C7	
QuadSi	20			C4	C8	

3.3 Characterization

Three different characterization methods were utilized on modified particles to control the quality of the final product. First, Fourier Transform Infrared (FT-IR) Analysis (Thermo Scientific Nicolet IS10) was performed in the transmission mode and at 1 Bar purged nitrogen gas for 1 hour to see the chemical effect of silane agents on the silica particles after chemisorption. Samples were prepared with a ratio of 2mg sample/200 mg KBr and under pressure of 9 Bar. Second, proton NMR ($^1\text{H-NMR}$) analysis was utilized with 500 MHz Varian Innova NMR and with samples in Deuterated chloroform (CDCl_3) to check whether or not the surface of fumed silica particles were covered with silane coupling agents, Third, thermo gravimetric Analysis (TGA) (Schmadzu DT_TGA) was performed to understand how much the silane coupling agent was adsorbed on the surface of silica particles. TGA analysis was done under a nitrogen environment with $10^\circ\text{C}/\text{min}$ heating rate.

In order to understand the degree of agglomeration in modified and unmodified silica particles and to measure the particle size of these particles, Transmission Electron Microscopy (TEM) (Tecnai G2 F20 S-TWIN) was utilized with copper grids that were covered with the samples. Another microscopy analysis, cryo-TEM (FEI Company Tecnai, G2 Spirit BioTwin) was utilized to characterize the dispersion of particles as well as particle radius in continuous medium. Suspensions were diluted in ethanol with 1/10 ratio, they were transferred onto the formaldehyde grids and after that ethanol was removed from samples. Scanning electron microscopy (SEM) (1530 Gemini LEO, Zeiss) was utilized to see the microstructure of particles used in this study.

To determine the hydrodynamic radius of particles in the suspensions, the Dynamic Light Scattering (DLS) (Nano Zeta Sizer, Malvern) technique was utilized with a disposable polystyrene cuvette filled with ethanol at a dilution ratio of 1/10, 1 being the sample; 10, the pure ethanol.

Steady and dynamic rheological analyses were utilized by using a rotational rheometer (Gemini II, Bohlin Inst.) at a controlled stress mode with a cone and plate geometry (2° cone angle and 40 mm). In order to remove any shear history from the samples, pre-shear at 60 s^{-1} for 10 seconds with a 10 seconds equilibrium time was applied. In experiments where electrical resistance measurements were simultaneously performed

with rheological measurements, the parallel plate was chosen over the cone and plate as the truncated geometry is unsuitable for electrical resistance measurements. The plate diameter is set to 40 mm so as to coincide with the results obtained from cone and plate geometry. Since the conductive particles (CNT and graphene) are susceptible to agglomerate, gap size was determined at 500 μm so as to be greater than the particle size in a particulate system; thus, accurate measurement could be obtained. Steady shear rheological analyses were performed with a shear stress range of 1-2000 Pa. In dynamic rheological analyses, strain sweep experiments were conducted for different frequencies to observe linear viscoelastic (LVE) and non-linear viscoelastic (non-LVE) zones. To observe microstructural change under low and high shear deformations, frequency sweep experiments were done with strain values from LVE and non-LVE region and in a frequency range from 0.628 rad/s to 628 rad/s. Constant frequency sweep experiments were utilized with 1.59 Hz frequency and 10 Pa dynamic shear stress to observe microstructural development with time. 1ks^{-1} pre-shear was applied for 5 seconds to break up all microstructure before the test. To understand the effect of temperature on viscosity and microstructure of the suspensions, temperature sweep experiments were conducted under constant steady shear (100 Pa) with a heating rate of $5^{\circ}\text{C}/\text{min}$ in a temperature range from 25°C to 125°C . Suspensions were also measured under constant frequency (1 Hz) and constant dynamic shear stress (100 Pa) with a heating rate of $5^{\circ}\text{C}/\text{min}$ in the same temperature range to characterize the microstructural change in the suspensions.

CHAPTER IV

4 RESULTS AND DISCUSSIONS

In this study, we aimed at investigating the parameters affecting the rheological behavior of suspensions containing agglomerated particles with low weight percentage. In the previous study performed by our group [37], some of these parameters (particle size, particle concentration, chain effect of continuous media) have been investigated. Here, we investigated the chemical and physical parameters of the particles, for example respectively the surface properties of the particles as well as the morphology of the particles and the temperature of the colloidal suspensions. To investigate the effect of these parameters on the rheology of the suspensions, a systematic characterization was designed as follows: *In section 4.1*, results for electrical resistance measurements that were performed simultaneously with steady shear rheological measurements were given to understand the phenomenon in shear thickening behavior of suspensions containing conductive nano particles. *In section 4.2*, rheological behavior of the suspensions containing particles with different morphologies (CNT, graphene, clay) has been discussed to explain the effect of morphologies on the shear thickening behavior. The findings were also supported with cryo-TEM images. *In section 4.3*, the rheological behavior of the suspensions containing modified silica particles covered with different silane agents was investigated; these discussions included not only steady shear rheological analysis but also dynamic rheological analyses so as to describe the particle-particle and the particle-polymer interactions in the suspensions containing surface modified silica particles. *In section 4.4*, the effect of temperature on the rheology of the suspensions was described. Then the study was concluded with final remarks.

4.1 Mechanism behind Shear Thickening Behavior

In this part of the work, the mechanisms behind the shear thickening phenomenon have been investigated by performing rheological and electrical resistance measurements to monitor the microstructural development in a given suspension. Towards this end conductive particles (CNT and graphene) were dispersed in a non-conductive medium (PEG) and then microstructural change has been monitored by utilizing the custom-made system described in details in *Section 3.2.1*. The reverse case, where non-conductive particles (fumed silica) were dispersed in a conductive medium (PEG200 became conductive by adding LiCl) has been investigated and discussed in the previous work performed by our research group [37]. In the previous work it was proven that; in shear thinning region, the conducting continuous media flows easily between adjacent silica flocs so the electrical resistance of the suspension does not change. At higher shear rates where the suspension experience shear thickening behavior; compacted flocs are broken down into small aggregates; increase in the surface area of non-conductive particles hinders the penetration of conductive polymeric chains due to higher tendency of particle interaction. Thus, electrical resistance of the suspension increases [37]. For all suspensions, first; electrical resistance measurements under stationary conditions were performed to observe the resistance of suspensions without applied shear forces. All measurements show that there is a drop in the resistance within the first 20-40 seconds. After this drop, electrical resistance plateaus.

Fig.4.1 shows the resistance of S4 (1 wt% graphene in PEG) suspension under steady shear together with viscosity profile. Since the particles are initially agglomerated and hence are in close contact with each other at their initial configuration, the suspension has a higher conductivity initially (9 kohm). The suspension shows three typical zones in its viscosity profile, which is commonly observed in shear thickening fluids. In the first region (0-40 s), the plateau in both viscosity and resistance profiles indicates that suspension exhibits a Newtonian behavior. In the second region, there is a sharp and sustained decrease in the viscosity due to the fact that the applied shear breaks down agglomerated discrete particles into small aggregates and these suspended aggregate particles are aligned in the direction of the flow due to the applied shear. Upon the breakage of agglomerated discrete particles, the entrapped polymeric liquids are released into the suspension, and particle-particle interactions are further reduced. Since

polymeric liquid adheres to the surface of the particles, which results in repulsive colloidal forces among particles, conductive particles will have a better dispersion in continuous media, leading to an increase in the resistance of the suspension and the decrease in the viscosity. At a critical shear rate, the particle ordering is disrupted and clumps of particles are formed which is referred to as the shear induced changes in the microstructure of the suspension. At this critical shear rate, a transition from shear thinning to shear thickening takes place since particles begin to interact in disordered manner, hence forming particle aggregation or a network structure whereby the electrical resistance decreases and the viscosity increase increases due to the increased particle-particle interaction.

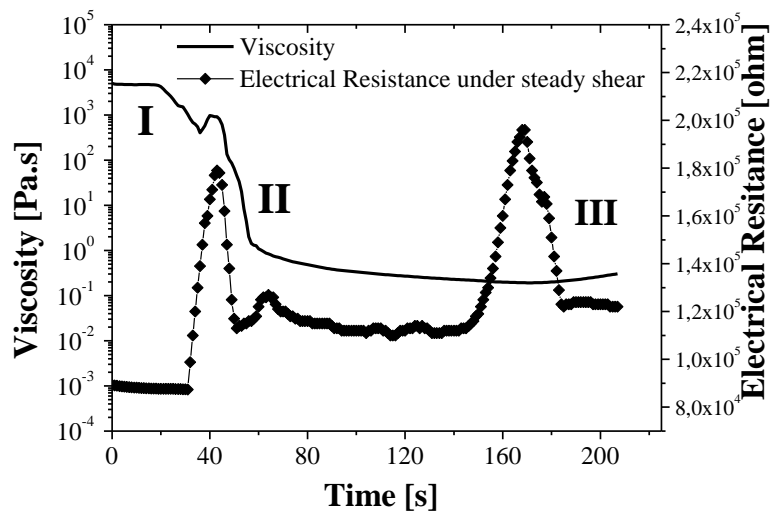


Fig. 4.1 Comparison of viscosity profile and resistance change in S4 (1 wt% graphene in PEG) suspension under shear forces with time

According to ODT theory; the particles begin to disperse well in shear thinning region when gradual shear forces are applied and the particles will have an ordered structure in continuous media due to enhanced dispersion. The sudden increase in the electrical resistance curve (Fig.4.1) in the second region meaning that particles are ordered, hence having less interaction. When the stress proceeds to increase, ordered structure has been disrupted. Since the system reaches to the critical stress value at which transition from shear thinning to shear thickening takes place, particles rearrange themselves; they begin to interact into disordered manner and constitute a network structure in shear thickening region. Brader [44] reported in his review that; hydrodynamic lubrication forces lead to particle clustering at high shear rates; hydrodynamic contributions to the viscosity is enhanced due to cluster formation which results in shear thickening behavior. Cluster formation induces the transition from ordered to disordered state;

sudden decrease in the electrical resistance curve (Fig.4.1) at 175s explains explicitly this transition.

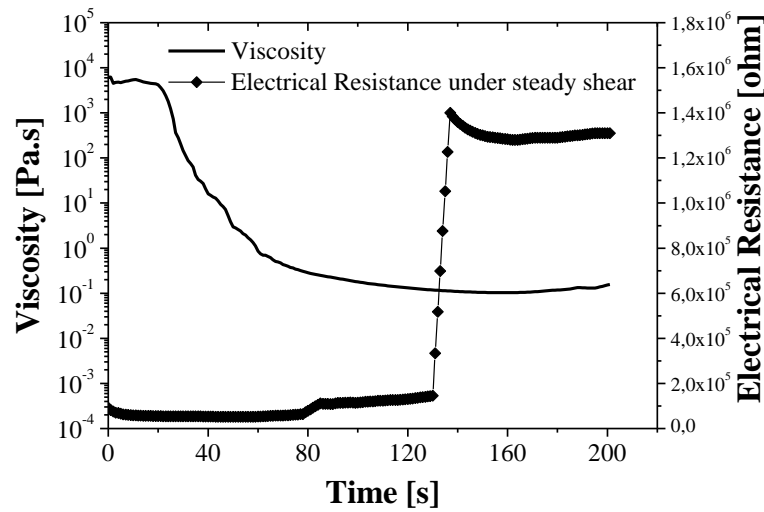


Fig. 4.2. Comparison of viscosity profile and resistance change in S1 (1 wt% CNT in PEG) suspension under shear forces with time

Same experiment protocol was repeated with another conductive particle, CNT, which has the same weight percentage with S4. For S1 (1 wt% CNT in PEG) the resistance curve (Fig.4.2) is similar with the resistance curve belonging to S4 (Fig.4.1.). There is a rise in resistance with increasing shear rate; agglomerates are broken down into small aggregates by applied shear which enables the polymer penetrate into small sized aggregates. From the resistance curve (Fig.4.2.) one may conclude that the dispersion of particles in the continuous media results an ordered structure containing particles without interaction; so viscosity of S1 will decrease (Fig.4.2). However, when the S1 reaches to a critical point where an increase in viscosity happens, particles will again interact each other (percolation threshold); the resistance of the suspension will decrease sharply.

Simultaneous measurements for S5 (3 wt% graphene in PEG) and S2 (3 wt% CNT in PEG) suspensions (Fig.4.3.a and b respectively) also proof the microstructural development under applied shear forces. Both suspensions exhibit shear thinning behavior (Fig.4.3). Trend in their electrical resistance curves are also similar; there is an increase in electrical resistance with increasing shear stress regarding to microstructural ordering of conductive particles without interaction (Fig.4.3). S5 and S2 are still in shear thinning region (2nd region). Barnes reported in his review article that; all

suspensions might exhibit shear thickening behavior under right conditions [2]. It is expected that, when high shear forces that are adequate to drive the particles into a disordered state, are applied, both S5 and S2 will also show shear thickening behavior. However; such high shear forces are not measurable in current commercial rheometer, thus shear thickening region was not monitored in S5 and S2.

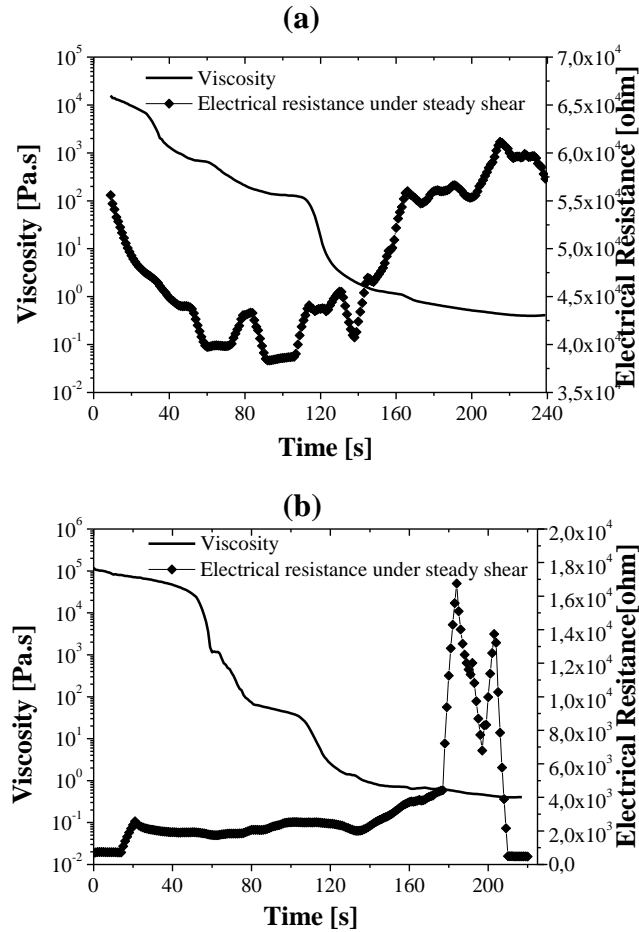


Fig. 4.3. Comparison of viscosity profile and resistance change in (a) S5 (3 wt% graphene in PEG) and (b) S2 (3 wt% CNT in PEG) under shear forces with time

These experiments were also repeated with suspensions comprising mineral oil as a continuous phase. The reason to choose the mineral oil is that, mineral oil has a non-polar structure and composed of long chain C atoms. Better dispersion for CNT and graphene particles is achieved due to the chemical structure compatibility with the continuous phase. Electrical resistance measurements simultaneously performed with rheological analysis for S11 (3 wt% graphene in mineral oil) also shows that there is a sudden resistance drop in the shear thickening region (Fig.4.4.b) where the conductive particles constitute a network structure due to the disruption of particle ordering. In

shear thinning region; agglomerates are broken into small aggregates. At the same time, mineral oil that was trapped into aggregates comes out. Continuous phase generates a lubrication effect on the particles. From TEM image (Fig.4.4.a), it is also seen that suspensions comprise mineral oil as a continuous phase have better particle dispersion.

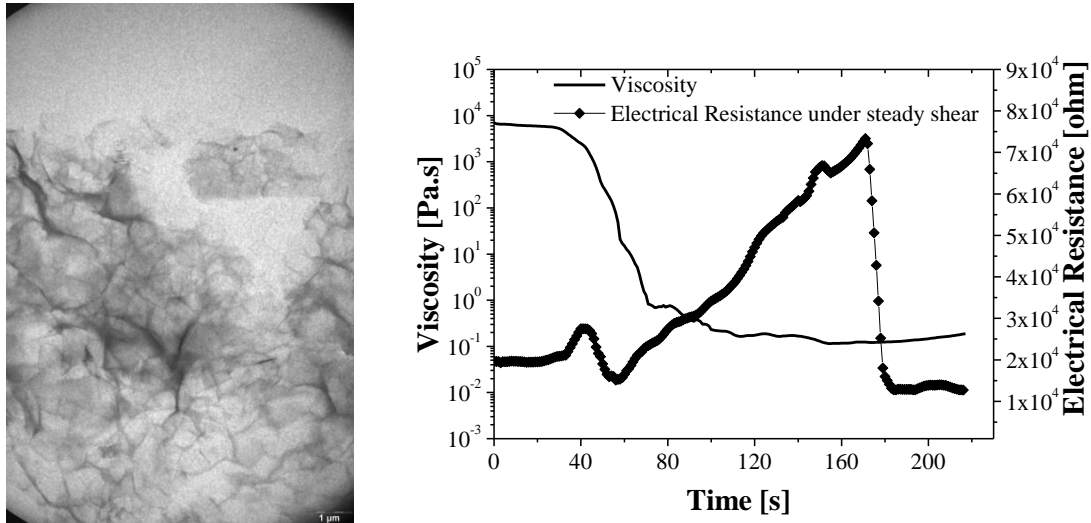


Fig. 4.4. (a) cryo-TEM image and (b) resistance measurement with viscosity for S11 (3 wt% graphene in mineral oil)

4.2 Particle Morphology Effect

Particle morphology, particle shape and size affect the rheological behavior of polymeric suspensions. Particle morphology can alter the rheological behavior from shear thinning to thickening vice versa [4]. With this regard, particles with different morphologies have been studied. To do so, halloysite, Na-bentonite, organoclays as montmorillonite clay (NMT4100) and, nanoclay, CNT and graphene were selected as particles in this study. The weight fraction of the particles in the liquid phase is chosen to be 20%. However, suspensions containing CNT and graphene could not be prepared as having 20% weight fraction due to their high agglomeration affinity [45] which hinders the dispersion in continuous media. Thus, for the sake of the consistency particle weight fraction is chosen to be 5% for silicate based materials as well in this section.

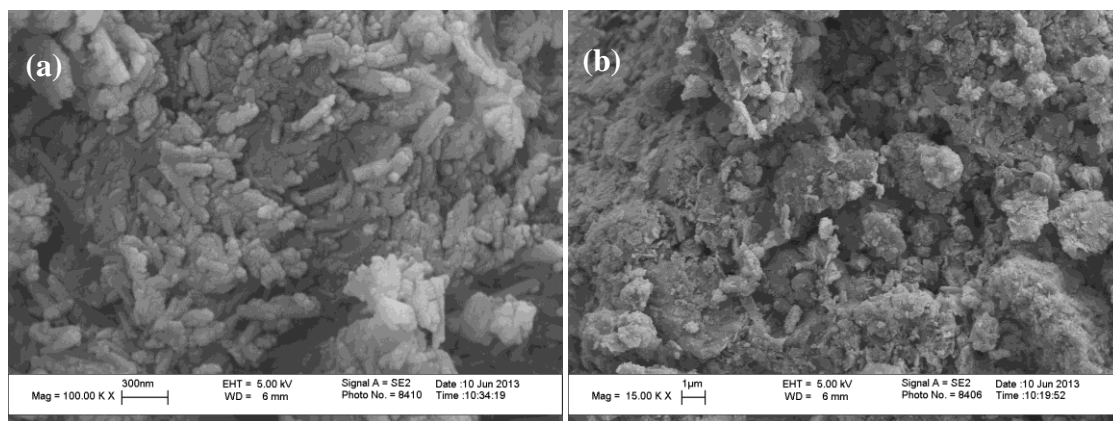


Fig. 4.5. SEM micrographs of (a) halloysite (b) Na-bentonite

SEM micrograph for silicate based materials, halloysite and Na-bentonite is given in Fig.4.5. Halloysite has a tubular structure with a diameter in the order of 100 nm while Na-bentonite, purified clay without modification, has a platelet or “layered” structure having thickness in the order of nanometer and length in the order of micron size. The particle size for halloysite and Na-bentonite was measured as 130 nm and 463 nm with DLS technique respectively. Upon the examining of viscosity profiles for S14 (5 wt% halloysite in PEG) and S15 (5 wt% Na-Bentonite in PEG) in Fig.4.6, both S14 and S15 exhibit Newtonian behavior over a wide range of shear rate. The particles slide over in the direction of the flow of polymeric fluid; low degree of friction between particles will result in low viscosity. But the behavior of S14 deviates from linearity in some respects compared with the behavior of S15. The viscosity value of these suspensions is in the order of approximately 0.07 Pa.s for S14 and 0.06 Pa.s for S15 respectively. Those viscosity values are close to the viscosity of continuous media (0.056 Pa.s) which might be contributed to the large particle size of as received Na-bentonite clay. Small surface area is leading to less effective volume fraction of particles under shear which results in a Newtonian behavior. For S14 (5 wt% halloysite in PEG), the reason for the Newtonian behavior might be happened regarding the exfoliation of halloysite layers with polymer. When the DLS results for S14 and S15 are examined, hydrodynamic radius (HR) is in the order of 900 nm for S14 and in the order of 1200 nm for S15 respectively. This finding is also another reason why S15 have Newtonian behavior. At higher critical shear rates ($> 2 \text{ ks}^{-1}$), shear thickening behavior is observed in S14 and drastic change in viscosity takes place at post shear rate values (17 ks^{-1}). However, this drastic increase might be observed regarding the spreading the sample out under high shear rates; less amount of sample has a less surface area thus cause an increase in the

viscosity. To verify the shear thickening behavior in S14 and S15 as well to monitor the microstructure of those suspensions during flow, small amplitude oscillatory shear (SAOS) and large amplitude oscillatory experiments (LAOS) experiments were utilized as a mechanical spectroscopy.

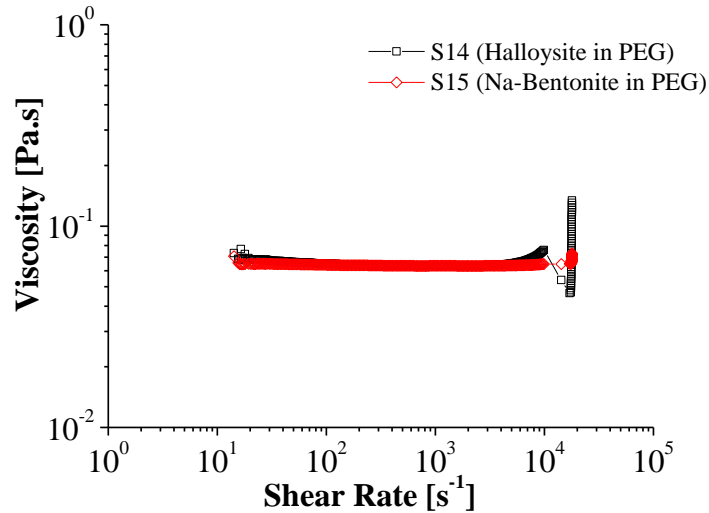


Fig. 4.6. Viscosity profile of S14 and S15

The linear viscoelastic behavior of S14 and S15 in Fig.4.7 shows that G' and G'' of S14 as well as S15 exhibit dependency on frequency. However, elastic modulus (G') is greater than viscous modulus (G'') in S14 (5wt% halloysite in PEG) for the entire range of frequency. The non-linear behavior in the viscosity of S14 in Fig.4.6 might be attributed to this fact as well. At higher frequencies (> 100 rad/s for S14 and >300 rad/s for S15 respectively), increase in the complex viscosity is observed in each of two suspensions which verify the shear thickening behavior of S14 and S15. The linear behavior in the complex viscosity of S15 over a wide range of frequency might also explain the Newtonian behavior of the viscosity under steady shear forces. According to Cox-Merz rule, viscosity profiles of Newtonian fluids under steady shear overlap with profiles under dynamic shear [46].

The results of LAOS experiments for S14 as well as S15 in Fig.4.8 also justify the shear thickening behavior of those suspensions. Critical frequency where the viscosity begins to increase shifts to pre-frequency values in S15 (5 wt Na-Bentonite in PEG)

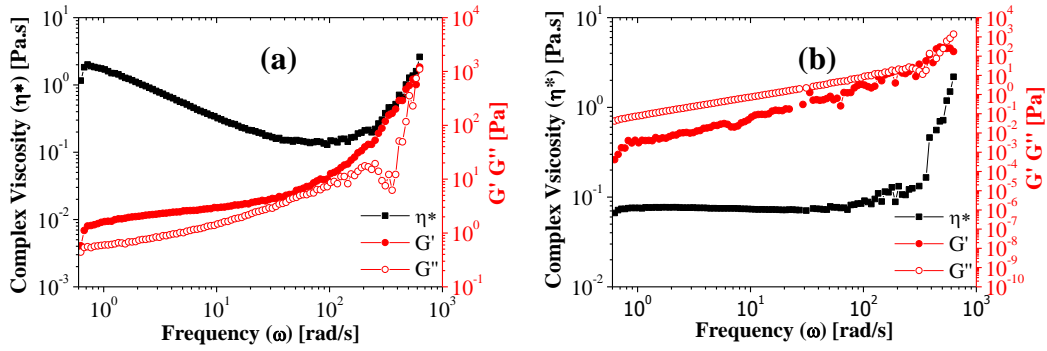


Fig. 4.7. Mechanical spectroscopy of **(a)** S14 (5 wt% halloysite in PEG) and **(b)** S15 (5 wt % Na-bentonite in PEG) in LVE

regarding the increase in the G' . The increase in the G'' of both S14 and S15 indicates energy loss in the material due to the friction between particles under rising shear field. It might be concluded that both S14 and S15 exhibit shear thickening behavior under large deformations although they exhibit Newtonian behavior over a wide range of shear rate under steady shear.

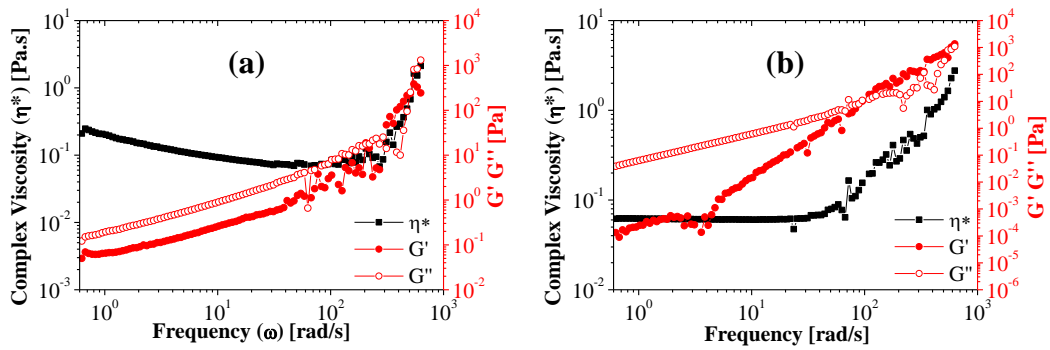


Fig. 4.8. Mechanical spectroscopy of **(a)** S14 (5 wt% Halloysite in PEG) and **(b)** S15 (5 wt% Na-bentonite in PEG) in non-LVE

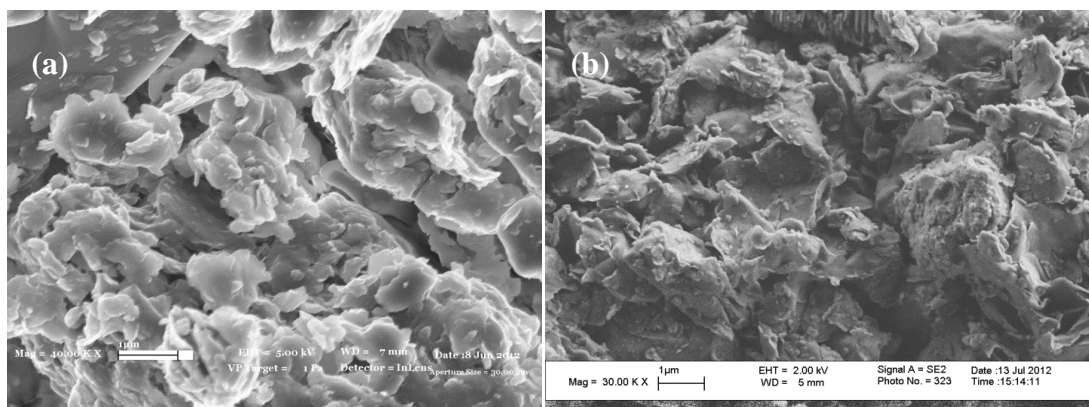


Fig. 4.9. SEM micrograph (scale bar: 1 μm) for **(a)** NMT4100 clay and **(b)** Esan nanoclay

Microstructure for both NMT4100 clay and nanoclay is given in Fig.4.9. These organoclays are composed of a two dimensional layered structure with micron size length and nano size thickness that is confirmed by SEM images. The size of these organoclay particles was measured as 1132 nm and 450.8 nm for nanoclay and NMT4100 clay respectively by DLS measurements. When the viscosity profiles of S19 and S15 in Fig.4.6 are examined both suspensions exhibit shear thickening behavior at higher shear rates (17 ks^{-1}). The initial viscosity of S19 at low shear rates (0.009 s^{-1}) is higher than S17. This result is the evidence of agglomerated particles in the suspension at initial state a result which is also supported by DLS measurements. A hydrodynamic radius of organoclays in PEG was measured as 320.7 nm with a PDI value of 1.000 and as 273,6 nm with 0.091 PDI for S19 and S17 respectively. Anisotropy in particles induces the increase in the viscosity; random distribution of silicate layers at low shear rates results in high viscosity. Recall that as stated in *Section 4.1*, aligning silicate layers will be aligned towards the direction of flow which will result as a decrease in the viscosity. The organoclays in those suspensions are exfoliated and the exfoliation increases the friction between the silicate layers [47] thus, at high shear regime viscosity increase is observed due to the fact that diminishing the lubrication of polymeric fluids between layers leads to friction between the silicate layers as well as the exfoliation induced friction will result in an increase in the viscosity of S17 and S19.

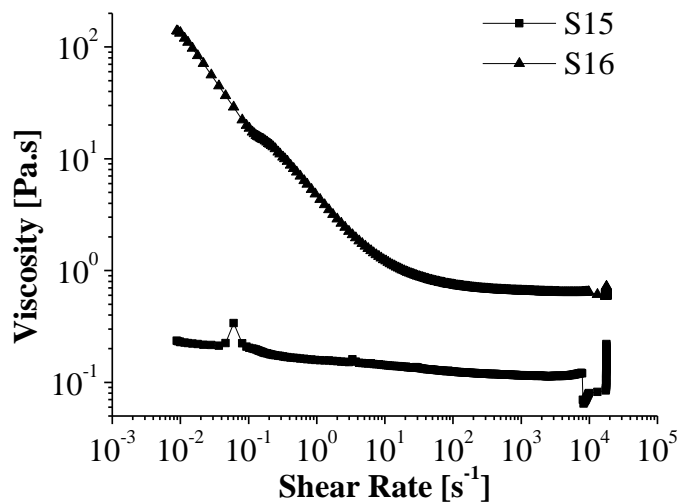


Fig. 4.10. Viscosity profile for S15 (20 wt% NMT4100 clay in PEG) and S16 (20 wt% Nanoclay in PEG)

Dynamic shear experiments were performed in LVE (Fig.4.11) and non-LVE region (Fig.4.12 and Fig.4.13) for further analysis of the microstructure at equilibrium state as well at deformed state respectively. As stated in *Section 2.3*, analysis in the non-LVE zone mimics a similar behavior with steady shear experiments at high shear regime; however, the ones in LVE zone explain the behavior at low shear regime. In order to monitor the microstructure of suspensions at the equilibrium state, In Fig.4.11 are represented the frequency sweep results under dynamic stress values that are taken from the LVE region, which are plotted as the graphs of complex viscosity, G' (elastic modulus) and, G'' (viscous modulus) versus increasing frequency. S16 and S15 have solid-like character at low deformation frequencies due to the fact that $G' > G''$ as shown in Fig.4.11 a and b. Greater elastic modulus of S16 compared with S15 at low deformation frequencies (0.7- 1 rad/s) can explain the high initial viscosity of S16 in steady shear test in Fig.4.10. The increase in the complex viscosities of S15 and S16 is the sign of the shear thickening behavior in the mentioned suspensions at large deformation frequencies.

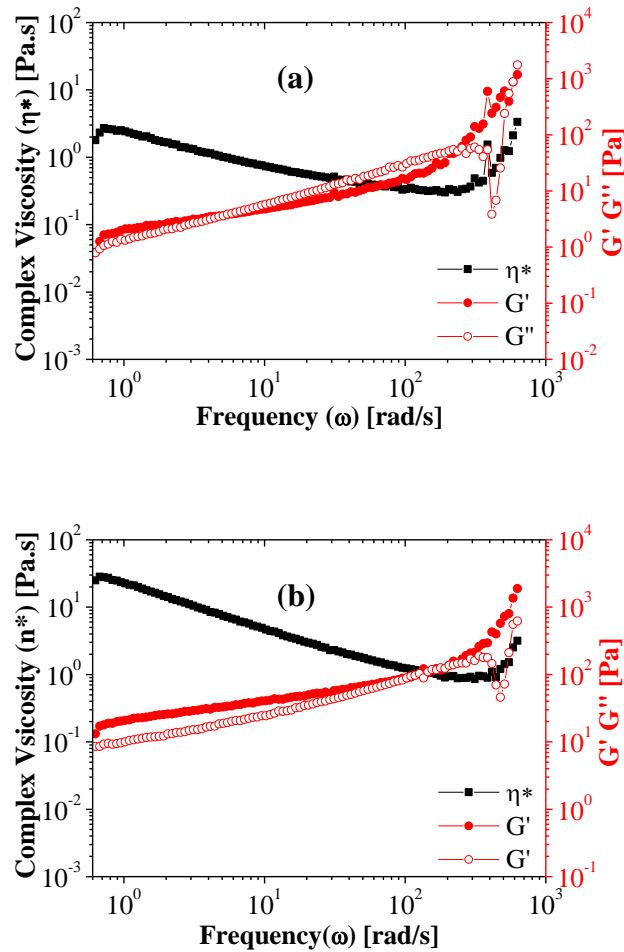


Fig. 4.11. Dynamic rheological analysis for (a) S19 (20 wt% Nanoclay in PEG) and (b) S17 (20 wt% NMT4100 clay in PEG) in LVE

In order to define the linear and non-linear viscoelastic region under varying deformation frequencies a strain sweep test was utilized, and the results (Fig.4.12) for S19 and S17 show that strain hardening occurs in elastic modulus after a critical point that is called critical strain. This point shifts towards to a smaller strain value as the frequency of deformation increases. Fig.4.12.a and b further indicate that the degree of shear thickening behavior increases in S17 as well as in S19 while the critical strain decreases. The breakdown of the internal microstructure induces the increase in elastic modulus with increasing angular frequency; the increase in the elastic modulus is associated with change from flocs to aggregated structure. Furthermore, strain dependency of elastic modulus (G') is a sign of flocculation in the structure [48]

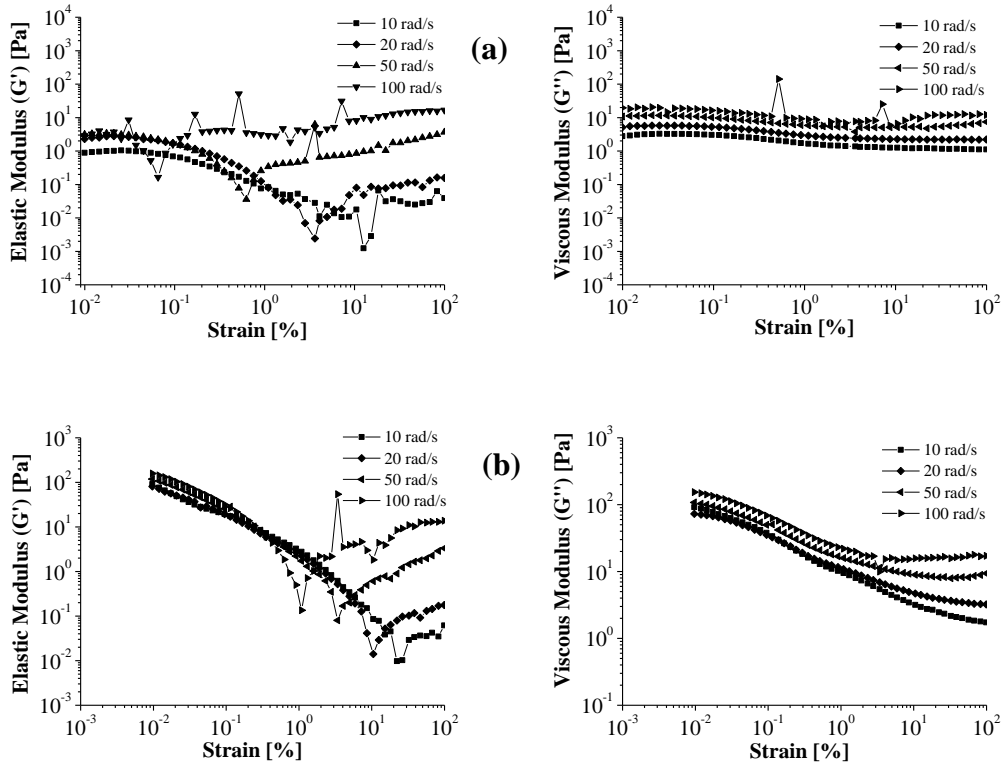


Fig. 4.12. Strain sweep results for (a) S19 (20 wt% Nanoclay in PEG) and (b) S17 (20 wt% NMT4100 clay in PEG) with varying deformations frequencies.

as well as the instability of the system [49]. Strain dependency of both S16 and S15 is the sign of flocculation; however, strain sensitivity is low in S16 compared with S15. This lower sensitivity can be attributed to the degree of flocculation in the suspension. G'' exhibit a linear behavior at high strain values for S16 and S15 as the degree of deformation increases. This is due to the fact that dissipated energy by viscous forces becomes constant since the interactions between continuous phase and discrete phase units dominate over the interactions between continuous phase and discrete phase, a process which in turn enables dispersion.

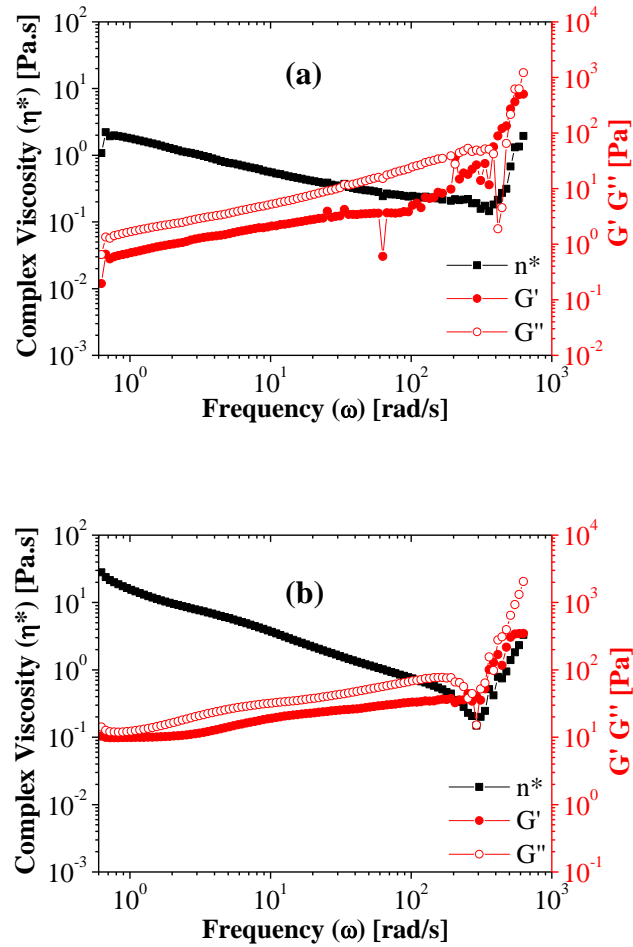


Fig. 4.13. Dynamic rheological result of (a) S19 (20 wt% Nanoclay in PEG) and (b) S17 (20 wt% Nanoclay in PEG) (under 0.1 strain)

Frequency sweep test results under LAOS stress of S16 (20 wt% Nanoclay in PEG) and S15 (20 wt% Nanoclay in PEG) are given in Fig.4.13.a and b. When the viscoelastic behavior of each of two suspensions is examined, their long term behavior (at low frequencies) is liquid-like because $G'' > G'$. At high frequencies which mimics the short term behavior of the system, both S16 and S15 show solid-like behavior regarding the increase in elastic modulus. Recall that LAOS measurement reflects a similar behavior in steady shear analysis under high shear stresses, the increase in the complex viscosity also reflects the shear thickening behavior in S16 and S15 after critical shear rate under steady shear forces.

For the consistency in terms of particle fraction, suspensions with organoclay particles were prepared having 5 % weight particle concentration and the rheological behavior of clay and organoclay suspensions were examined under steady and dynamic shear

forces. The viscosity profiles of Na-clay (Na-Bentonite) and organoclays (Nanoclay and NMT4100 clay) are given in Fig.4.14

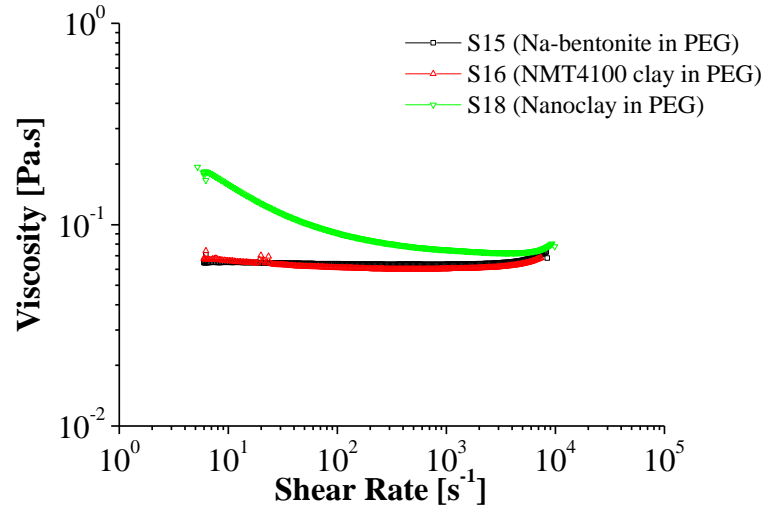


Fig. 4.14. Viscosity profile of S15 (5 wt% Na-Bentonite in PEG), S16 (5 wt% NMT4100 clay in PEG) and S18 (5 wt% nanoclay in PEG)

The viscosity profile of S16 slightly differs from profile of S15; they exhibit Newtonian behavior over a wide range of shear rate while S18 exhibit shear thinning. An increase in the viscosity at shear rates greater than 10 ks^{-1} is observed in those suspensions that can be seen in Fig.4.14. Higher initial viscosity (0.18 Pa.s) of S18 might be contributed to the greater hydrodynamic radius (700.00 nm) of Nanoclay particles in PEG. The PDI value of S18 is also high; 0.700 compared to the value of S16; 0.560. Polydispersed particles which also exhibit anisotropy will lead to a decrease in the viscosity as they are subjected to shear. Decrease in the viscosity happens due to the rolling of large particles on smaller particles. Steady shear experiments were not being performed at higher shear stresses ($> 1 \text{ kPa}$). Low viscosity fluids can easily escape underneath the plate of rheometer at high speed rotation. Thus reliable data for shear thickening could not be obtained for those S15, S16 and S18 as in the case of S14 (halloysite in PEG). Frequency sweep experiments were further performed for S16 (5 wt% NMT4100 in PEG) and S18 (5 wt% Nanoclay in PEG) so as to examine the rheological behavior under high shear forces. Upon the examining of the linear viscoelastic behavior of S16 and S18 from Fig.4.15, shear thickening behavior is observed at post deformation

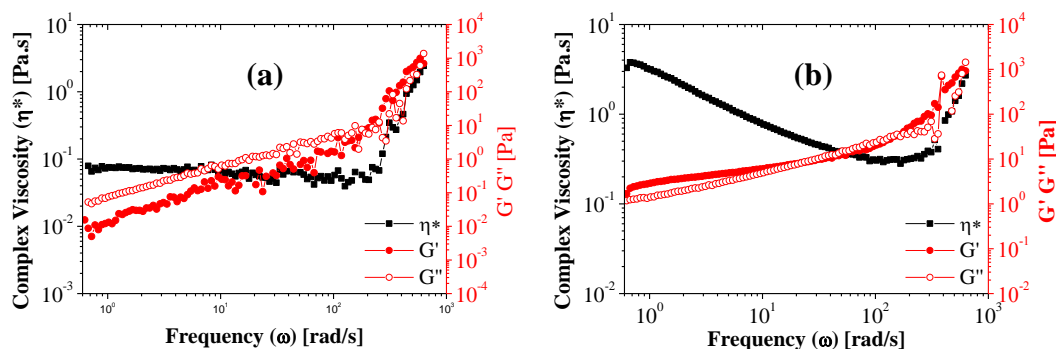


Fig. 4.15. Dynamic rheological result of (a) S16 (5wt% NMT4100 clay in PEG) and (b) S18 (5wt% nanoclay in PEG)

frequencies. Linear behavior in complex viscosity of S16 is observed until the critical frequency where the transition from liquid to solid-like structure takes place. The linear behavior of dynamic viscosity in S16 complies with that of behavior in steady shear analysis in Fig.4.14. Recall that same behavior was observed in the dynamic analysis of S15 (5 wt% Na-Bentonite in PEG) in Fig.4.7 and 4.8.

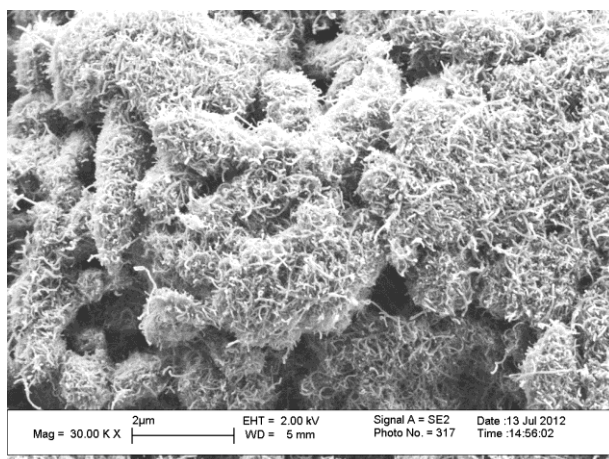


Fig. 4.16. SEM micrograph (scale bar: 2 μm) for CNT that was used in this study

The SEM image for CNT that is used in this study is given in Fig.4.16. These particles are composed of a high amount of agglomerated structures. Agglomeration hinders the dispersion of particles in continuous media efficiently and results for a low weight particle fraction suspensions to be prepared. Majumdar et. al. report that CNTs cause viscosity increase in dilute suspensions and they show shear thickening behavior [50]. Weight fractions of CNTs for suspensions S3 (5 wt% CNT in PEG) and S13 (10 wt% CNT in PEG) are higher than the values in several studies [39, 51, 52]; however, these suspensions show shear thinning behavior (Fig.4.17.a and b) at even higher shear

stresses (10 kPa). Rigid and bigger size flocs exist at initial state in the internal structure of the suspension due to the strong inter-particle interactions (van der Waals forces) between CNTs. The higher viscosity of S3 and S13 at low shear rates can be attributed the large amount of agglomerates in these suspensions a finding which is also confirmed by TEM images in Fig.4.18. The sustained decrease in the viscosity occurs because of the breakdown of large sized agglomerates into small sized isolated aggregates by applied shear and the entrapped polymeric fluid is released whereby the viscosity of the suspension decreases.

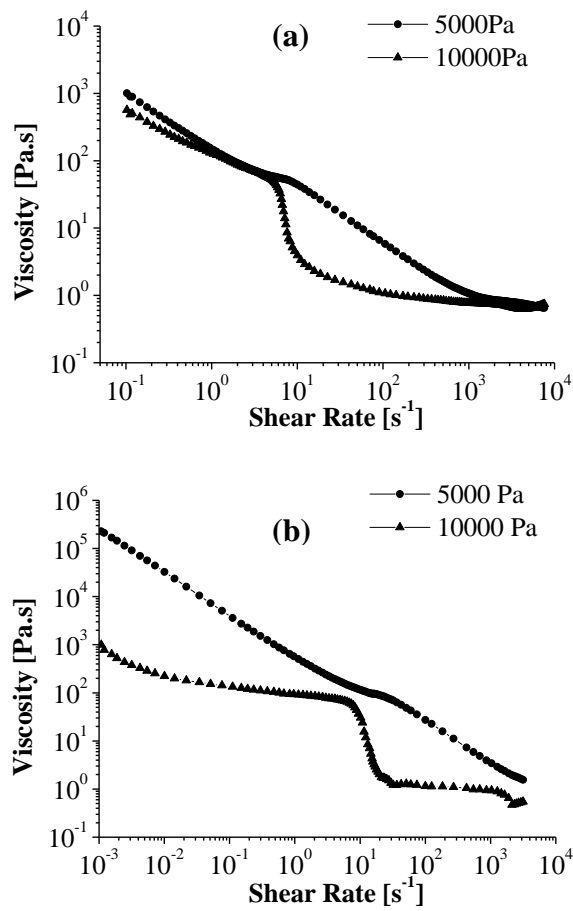


Fig. 4.17. Viscosity profile for (a) S3 (5 wt% CNT in PEG) and (b) S13 (10 wt% CNT in PEG) at 5k and 10 kPa max. shear stresses

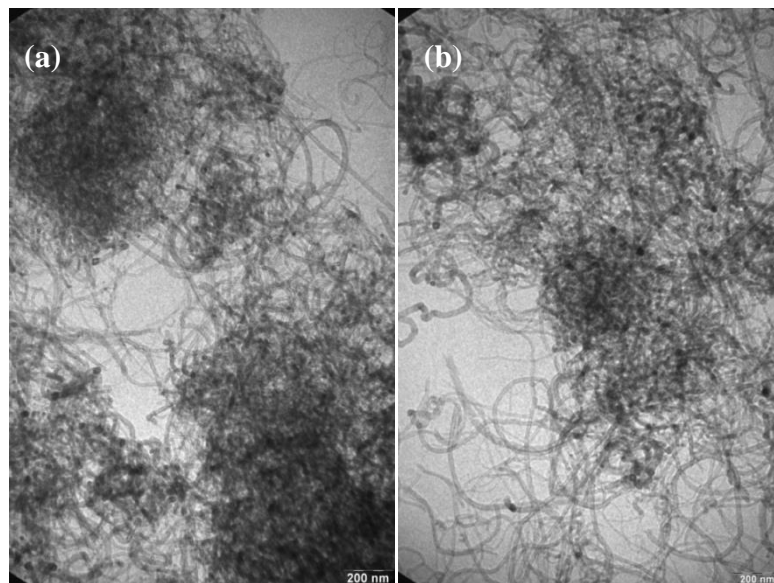


Fig. 4.18. cryo-TEM images (scale bar: 200 nm) for CNT filled PEG suspensions; **(a)** S3 and **(b)** S13

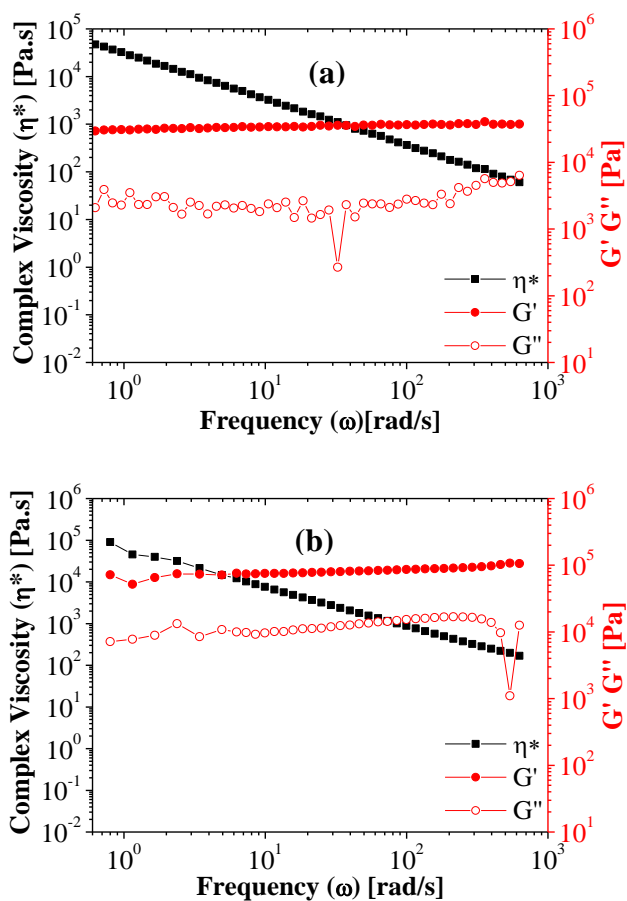


Fig. 4.19. Frequency sweep analysis of **(a)** S3 (5 wt% CNT in PEG) and **(b)** S13 (10 wt% in PEG) in LVE region

For further analysis of the microstructure of the suspensions, a frequency sweep test was performed under constant strain value which was taken in the linear viscoelastic region. Complex viscosity of S3 (Fig.4.19.a) also shows shear thinning behavior at high frequencies. The plateau of storage (elastic) modulus for whole frequency range is an evidence of agglomerated particles [51]. The sufficiently strong attractive particle interactions (van der Waals interactions due to the electronic structure of CNTs) between the discrete phase are attributed to the linear behavior of G' which develop more rigid and big sized flocs in the suspension since the rigid size flocs have higher resistance to motion under applied stress. The large elastic modulus (G') compared with viscous modulus (G'') also explains the high initial viscosity and shows that suspension has a gel-like structure at equilibrium. The same rheological behavior with S3 (Fig.4.19.a) in the LVE region is also shown for S13 (Fig.4.19.b). For the entire range of frequency sweep; viscosity decreases with increasing frequency. G' value is also constant in S13 for the whole range of frequency which again shows that particles are highly agglomerated in the continuous medium. Due to the high aspect ratio (which induces anisotropy) of CNTs (> 50) compared to other anisotropic particles (organoclays, diatomite, and so on.) studied in this section, they are most promising ones to cause shear thickening behavior. However, neither steady shear nor dynamic shear experiments were able to monitor the shear thickening behavior. Barnes reported that all suspensions exhibit shear thickening behavior under the right conditions [2]. Shear forces were not sufficiently enough applied to the S3 and S13 to break down big size agglomerates to finely dispersed aggregates due to the limitations of the equipment. For that reason, it is expected that they exhibit shear thickening behavior.

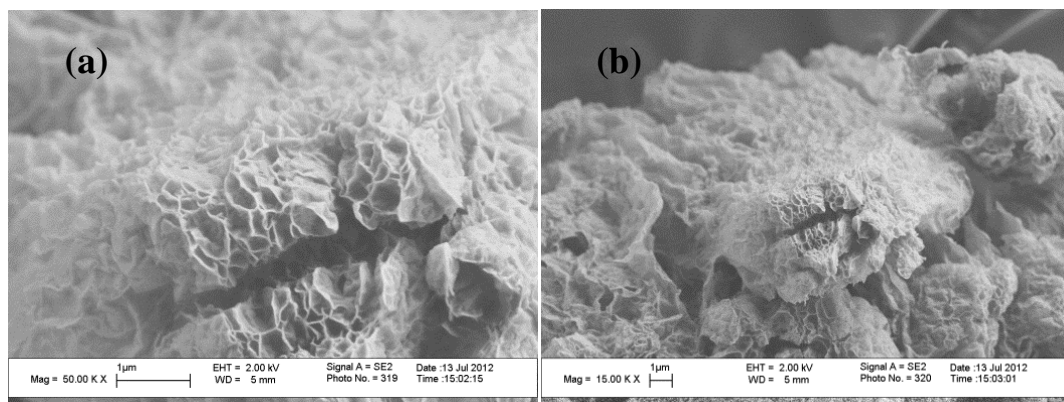


Fig. 4.20. (a) and (b) SEM images (scale bar: 1 μm) of graphene.

Lastly, flow behavior of graphene (composed of graphite layers, the SEM micrograph of in Fig.4.20) suspensions were investigated in *Section 4.2* and the initial viscosity of S6 (5 wt graphene in PEG) was measured greater than 1 kPa.s at low shear rates (0.01) under low shear forces given in Fig.4.21.a. The reason again is the big size flocs in the suspension which is confirmed by cryo-TEM images in Fig.4.21.c and d, due to the high interparticle interactions; however, in this case, the forces leading to the formation of agglomerates are depletion forces that cannot be prevented or screened in the suspension [42]. These attractive colloidal forces become weaker as the further increase of the shear stresses and the flocs are disrupted, then they turn into small sized aggregates. Therefore the viscosity of S6 (5 wt% graphene in PEG) will decrease due to the release of entrapped polymer molecules as shown in Fig.4.21.a. When the large amount of shear forces are applied (fig.4.21.b) to break down the agglomerates into fine sized aggregates initially, the viscosity will increase due to the high surface area of finely dispersed aggregates. Frequency sweep result of S6 in Fig.4.22 also support the shear thickening behavior

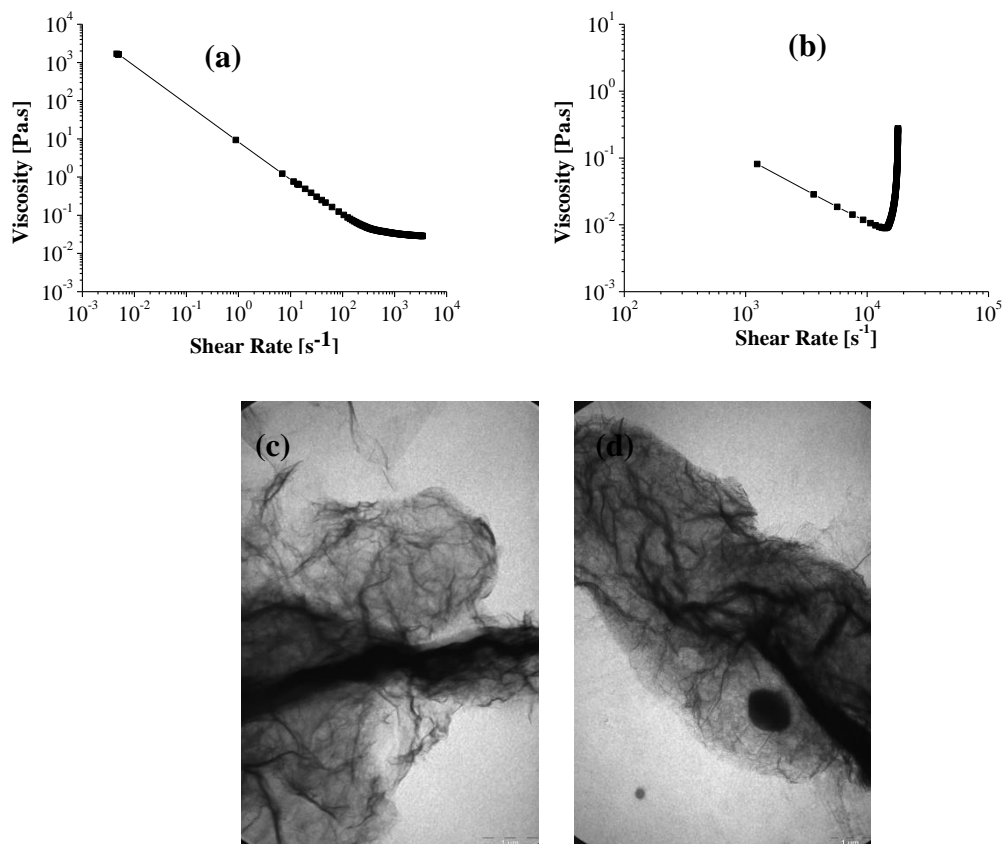


Fig. 4.21. Viscosity profile at (a) 100 and (b) 5000 max. shear stresses, (c) and (d) cryo-TEM images (scale bar: 1 μm) of S6 (5w% graphene in PEG)

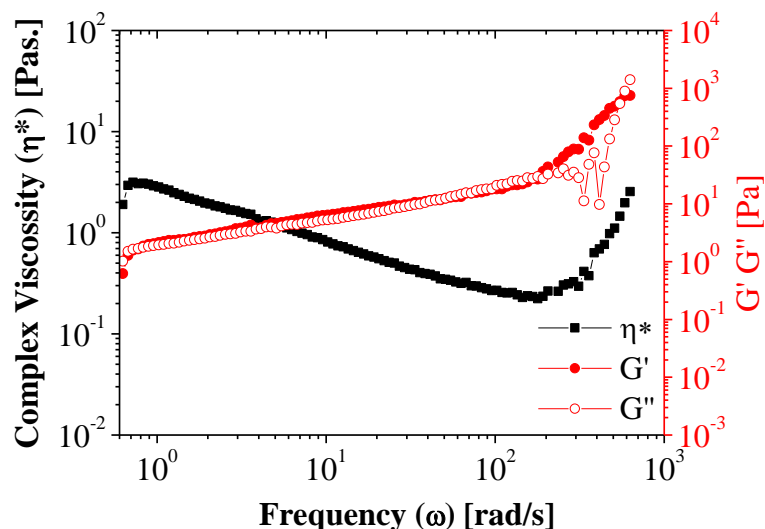


Fig. 4.22. Frequency sweep analysis of S6 (5 wt% in PEG) in LVE

4.3 Effect of Silica Surface Modification on the Rheology of Colloidal Suspensions

Surface properties of particles play an important role in controlling the rheology of nano particle suspensions. Particle-particle and particle-polymer interactions have strong affect that can lead to change in the rheological behavior from shear thickening to shear thinning vice versa [5]. For the case of silica particles; sol (stable solution) or gel (network structure) structures due to the H-bonding ability of continuous phase are formed [53]. In the light of these outcomes; in this section, surface of hydrophilic fumed silica particles were modified with three different silane agents to investigate the effect of surface properties. Results were discussed in two parts: 4.3.1. *Characterization of Modified Silica Nanoparticles* and 4.3.2. *Rheological Analysis* of the colloids containing modified silica particles.

4.3.1 Characterization of Modified Silica Nanoparticles

To be able to verify the chemisorption of silane agents onto the silica surface, FT-IR spectroscopy, ¹H-NMR spectroscopy and, thermogravimetric analysis were utilized

respectively. The results of regarding characterization methods are given in the following sections.

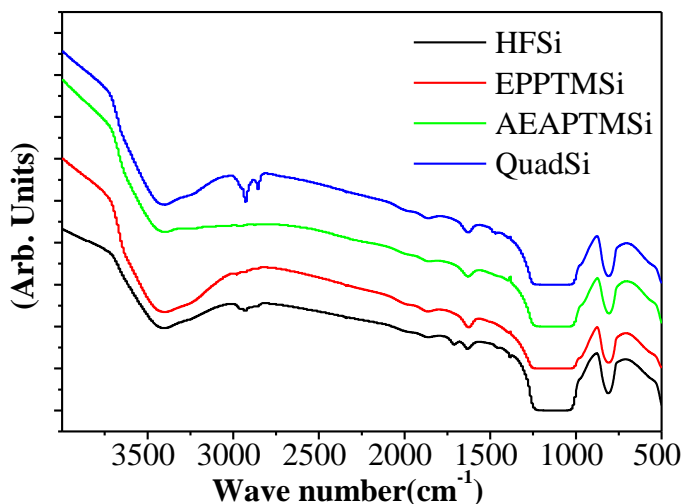


Fig. 4.23. FT-IR spectra for HFSi, EPPTMSi, AEAPTMSi, QuadSi

FT-IR spectra of HFSi and modified silica particles are given in Fig. 4.23. From Fig.4.23, it can be seen that, the peaks around 1130 and 810 cm^{-1} are absorption peaks of silica and belong to $-\text{Si-O}-$ group. This region refers to the fingerprint region for silica particles[35]. Indeed, the peaks around 3400 cm^{-1} belongs to $-\text{OH}$ groups in silica. In literature [34], it is mentioned that, peaks that are in finger print region do not alter for modified silica particles; there will be a minor shift in the peak around 3400 cm^{-1} due to the modification[34]. This minor shift is observed in spectra of modified silica particles. The $-\text{OH}$ groups belonging to the absorbed water on the silica particles arise at around 1633 cm^{-1} which also overlaps with free NH_2 in AEAPTMSi. Thus, free NH_2 groups were not detectable in the spectrum of AEAPTMSi. Other functional groups, NH in AEAPTMSi also overlapped with the $-\text{OH}$ groups of silica in 3400 cm^{-1} . From the FT-IR spectrum belonging to QuadSi (Fig.4.23), peaks around 2920 and 2850 cm^{-1} region indicates the long alkyl chain in quad silane agent's structure. Since the amount of absorbed silane agents is low, the major changes in functional groups in modified particles cannot be easily detectable in FT-IR spectroscopy. For that reason, $^1\text{H-NMR}$ analysis was further performed so as to verify the changes in the chemical structure of modified silica particles and the results are given in Fig.4.24

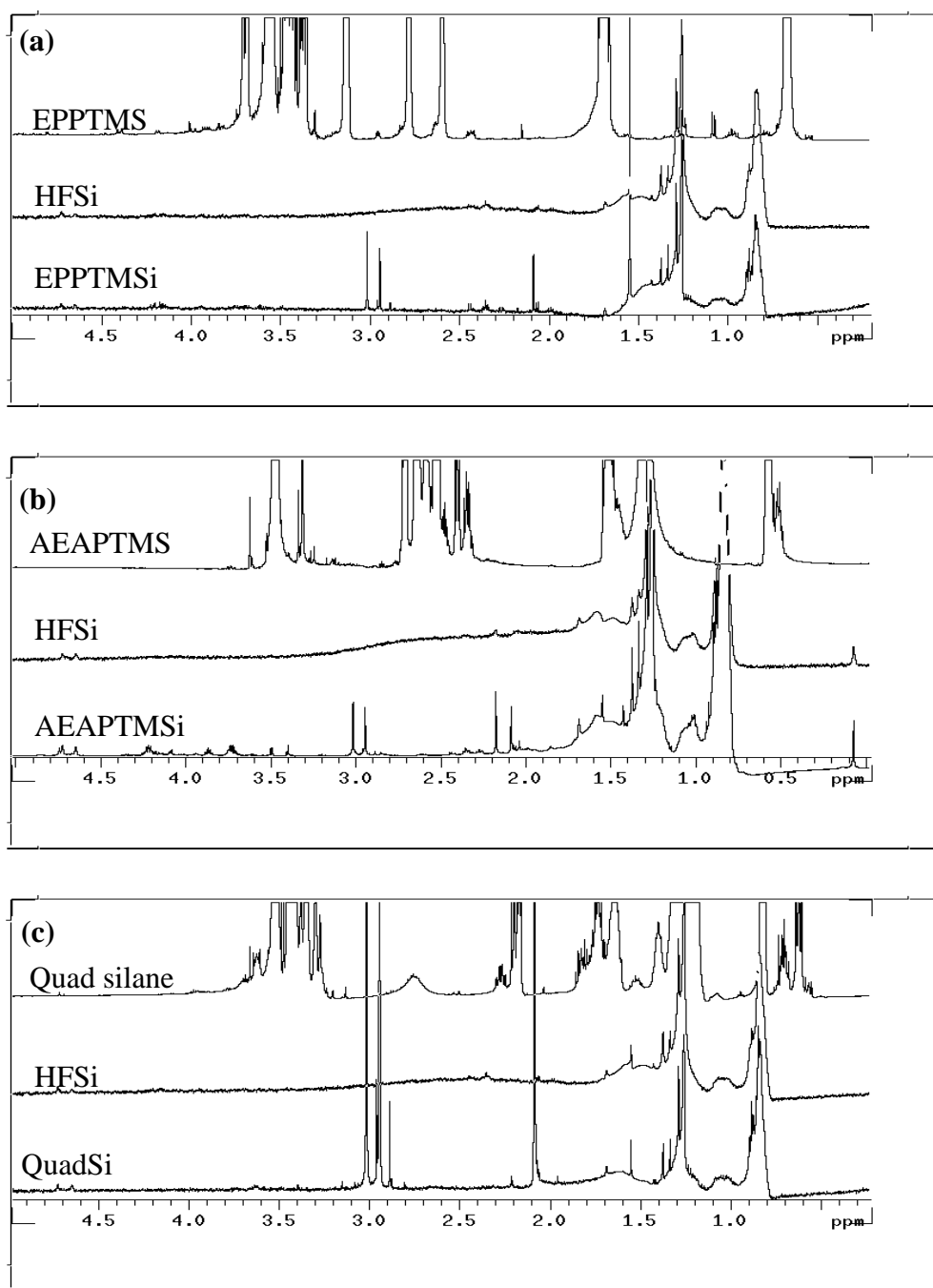


Fig. 4.24. Comparative ¹H-NMR spectra of silane coupling agents, fumed silica and modified silica particles respectively (a) EPPTMS-HFSi-EPPTMSi (b) AEAPTMS-HFSi-AEAPTMSi (c) Quad silane (quaternary ammonium compound)-HFSi-QuadSi

The comparative ¹H-NMR spectra of silane agents, fumed silica and modified silica particles are given in Fig.4.24 so as to evaluate the functional groups chemically adsorbed on the surface of silica particles. In the spectrum of HFSi given in Fig.4.24.a, b and c, the peak at 1- 0.8 ppm range arises from the isolated Si-OH bonds in HFSi structure, while the one around 1.3 ppm resembles the unbounded OH groups which signs the humidity on the particles. The ¹H-NMR spectrum of silane coupling agents

(first spectrum of comparative $^1\text{H-NMR}$ spectra in Fig.4.24.a, b and c) have a peak at 3.50-3.60 ppm regarding to the methoxy groups ($-\text{OCH}_3$) in their structure. Those groups are not observed in the spectra of modified silica particles (second spectrum of each comparative spectrum in Fig.4.24) which indicate that chemisorption was successfully taken place. Methoxy groups hydrolyze in ethanol and then the functional groups condense, make covalent bonding with Si. CH_2 groups bonded to Si have a peak at 0.62 ppm that is also seen in the spectrum of silane agents. However, this peak does not appear in modified silica particles, since this peak overlaps with the peak at 0.8 ppm. When 0-1.7 ppm range is considered as characteristic region (finger print region) of HFSi prominent changes are observed in 2.5-3.00 ppm range (Fig.4.24.a and b) and as well as in 3.00-5.00 ppm range (Fig.4.24.b) for modified silica particles. For EPPTMSi (Fig.4.24.a) the proton shifts at around 2.5 ppm and 2.9 ppm indicates the $-\text{CH}_2$ and $-\text{CH}$ groups in epoxy respectively. In the spectrum of AEAPTMSi (Fig.4.24.b); the peaks around 2-2.2 ppm might indicate the NH groups bonded to $-\text{CH}_2$ groups in the structure. The proton shifts at 3 ppm occur due to CH_2 groups bonded to amino groups. Upon examining the $^1\text{H-NMR}$ spectrum for QuadSi (Fig.4.24.c); the peaks at 3 ppm indicates the existence of the $-\text{CH}_3$ groups and the long alkyl chain ($\text{C}_{14}\text{H}_{29}$) bonded to N^+ functional groups.

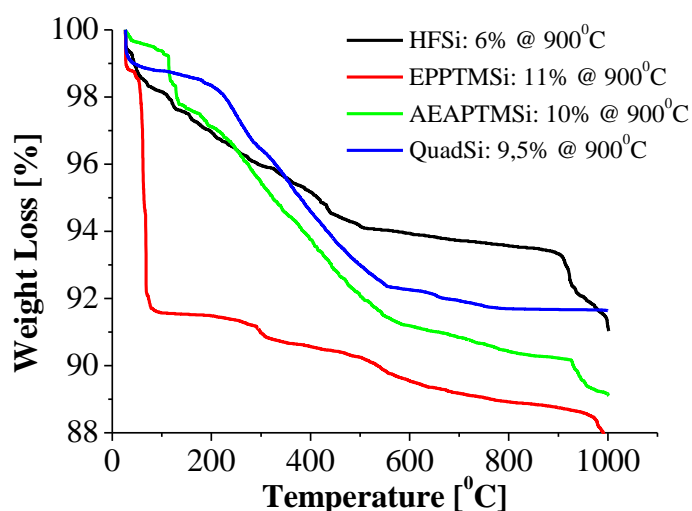


Fig. 4.25. TGA results of HFSi, EPPTMSi, AEAPTMSi, and QuadSi

The amount of silane coupling agents that is adsorbed on the surface of fumed silica particles was revealed by TGA and the results are given in Fig.4.25. The TGA curve for unmodified silica (HFSi) reveals that the weight loss of 2% at around 100°C comes

from the adsorption of physical water on the surface of the fumed silica. There is a gradual decrease in weight loss until reaching 500°C, when weight loss is at 6%. Weight loss is due to the degradation of surface silanol groups. For the case of the modified particles (Fig.4.25.), AEAPTMSi and QuadSi particles show a similar trend; there is also a weight loss, this time of approximately 100 °C. Weight loss occurs before 100°C due to the silane coupling agents. Under normal conditions, the weight loss due to physical water occurs at 100°C; however, in our work, the silane coupling agents shift this change before or after 100°C due to the chemistry of these agents. Weight loss at around 100°C in AEAPTMSi as well as in QuadSi is observed as 1%. For EPPTMSi, high amount of weight loss (8%) at around 100°C is observed in TGA curve in Fig.4.25. Large amount of water absorption on the surface represents the hydrophilic character of EPPTMSi particles compared to AEAPTMSi and QuadSi. 2% weight loss at approximately 200°C in TGA curve of AEAPTMSi happens due to the degradation of amine groups and other organic compounds. For QuadSi particles, the weight loss due to degradation of organic compounds takes place between 200 and 400°C and is an order of 3%. In the same temperature range, 1.5% weight loss was observed in TGA analysis of EPPTMSi.

Transmission Electron Microscopy (TEM) was also utilized to control the agglomeration as well as the size of the particles after modification. From the images in Fig.4.26 it might be concluded that silica particles have agglomeration tendency after modification as well. But, the modified particles exhibit diverse rheological behavior as well as colloidal interactions when they dispersed in polymeric media. These findings will be explained in details in *section 4.3.2*.

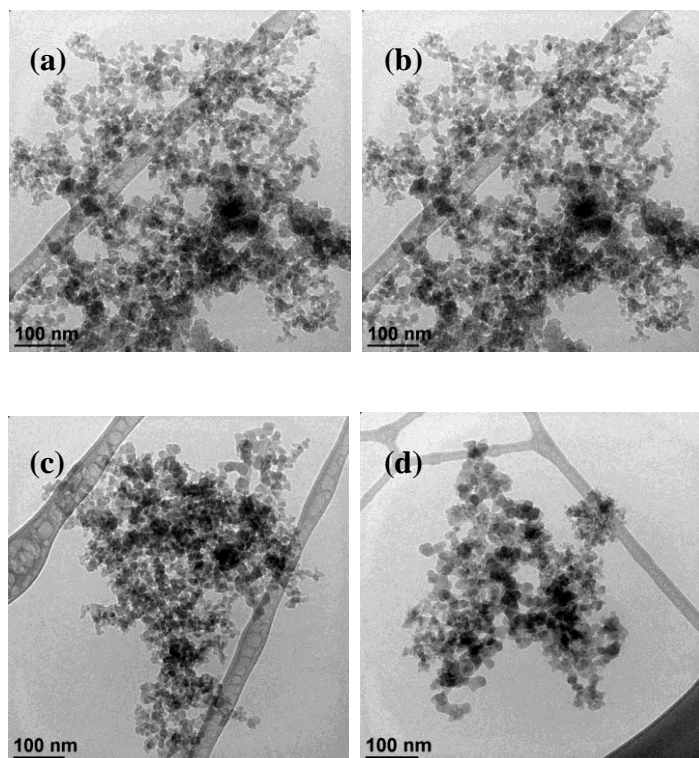


Fig. 4.26. TEM images of silica particles before and after modification: (a) HFSi (b) EPPTMSi (c) AEAPTMSi (d) QuadSi

4.3.2 Rheological Analysis

To address the influence of the surface properties of nanoparticles on the rheological behavior of colloidal suspensions, suspensions composed of particles with dissimilar surface chemistry and different polymeric media have also studied. Colloidal interactions in the suspensions as well as microstructural aspects were considered.

4.3.2.1 Steady Shear Analysis

The results of steady shear tests are given in Fig.4.27. Upon examining the viscosity profiles of C1 and C5, it can be seen that both C1 and C5 exhibit shear thickening behavior at low shear rates due to the hydrogen bonding capability of continuous media. However, in C1, the viscosity increase at the critical shear rate is sharp and distinctive in comparison to C5. This can be attributed to the stronger steric barrier in C1 than in C5 since the hydroxyl groups (-OH) on the PEG chain reacts with the surface hydroxyl of silica aggregates through forming hydrogen bonding, and leading to well dispersed

particles in the suspension. However, second hydroxyl groups in PPG chains (less reactive compared to those in PEG) are less prone to make hydrogen bonds with hydroxyl groups in fumed silica wherefore attractive van der Waals interactions among particles become dominant colloidal force. The alkyl group (CH_3) in the PEG chain also promotes the interparticle interactions. Higher interparticle interaction in C5 results in more agglomerates in the suspension, which is confirmed by DLS results such that the hydrodynamic radius of HFSi is 222.70 nm in PPG whereas it is 193.8 nm in PEG. Both C1 and C5 contain flocculated structures that are shown in cryo-TEM images as well as DLS results in Fig.4.28 and 4.29, respectively. The higher degree of agglomeration will

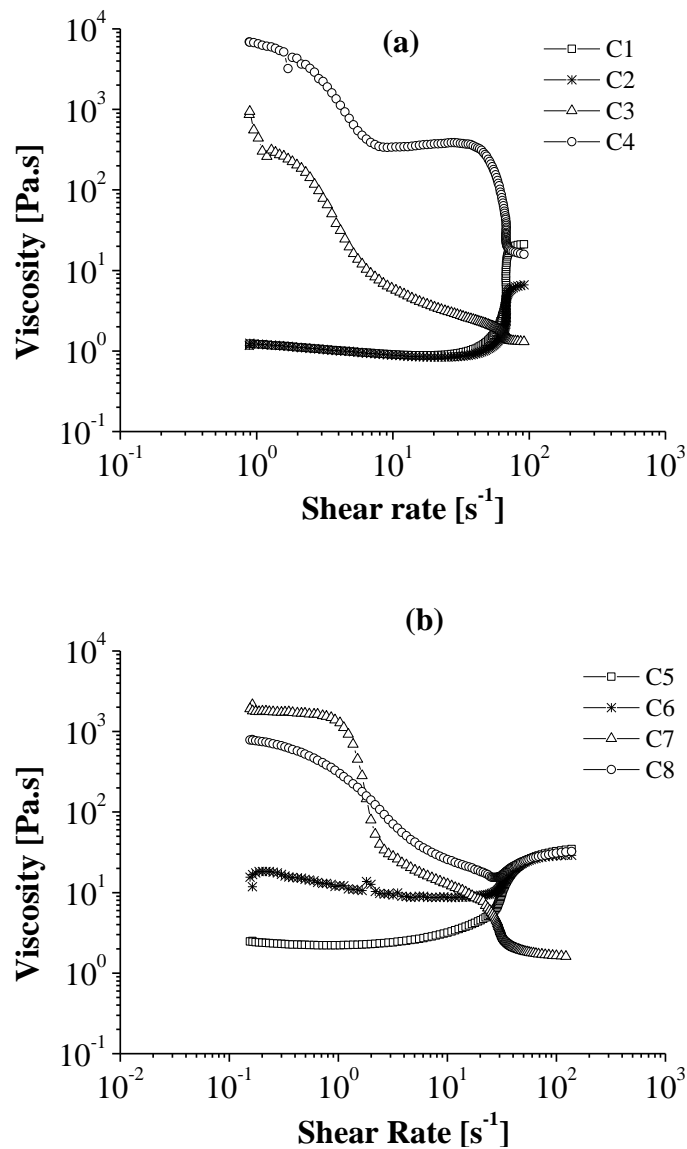


Fig. 4.27. Viscosity curves for unmodified and modified silica particles in (a) PEG and (b) PPG

prevent the formation of finely dispersed particles in continuous media.

The viscosity profiles of C2 (EPPTMSi in PEG) and C6 (EPPTMSi in PPG) show a trend similar to C1 (HFSi in PEG) and C5 (HFSi in PPG), meaning that both C2 and C6 exhibit shear thickening behavior at earlier (28 s^{-1} and 20 s^{-1} respectively) critical shear rates. While the viscosity profile of C2 (EPPTMSi in PEG) coincides with that of C1 (HFSi in PEG), C6 differs from C5 in terms of zero shear viscosity value. C6 has a zero shear viscosity (11.80 Pa.s) which is approximately 4.5 times greater than C5 (2.50 Pa.s). This might be attributed to the agglomerated particles in the suspension at initial state, which can be observed from cryo-TEM image (Fig.4.28.f). Epoxide groups in EPPTMSi make hydrogen bonding with hydroxyl groups in PEG and PPG since the oxygen atom in the epoxide structure promotes the interaction between particles and the polymeric media. Thus steric barrier forms around the particles and steric forces (repulsive forces) prevent agglomeration in the suspensions. However, the hydrogen bonding capability of C6 will be less due to the CH_3 groups as well as the less reactive OH groups in PPG chain. Relatively weaker interaction between polymer and the particles in C6 will result in larger hydrodynamic radius for particles (108 nm) compared to C2 (102 nm). To summarize, the attractive interparticle interactions in C6 cannot be weakened as much as the ones in C2 due to less hydrogen bonding capability of PPG, hence promoting agglomeration in C6. However, the size of agglomerates is small in C6 since the shear thickening behavior is observed in C6 as in the case of C2.

Suspensions C3 (AEAPTMSi in PEG) and C7 (AEAPTMSi in PPG) exhibit shear thinning behavior with high initial viscosities (861.8 Pa.s and 2150 Pa.s respectively) that can be seen in Fig.4.27.a and Fig.4.27.b and their viscosities show sharp decrease at low shear rates (4 s^{-1} and 1.5 s^{-1}). AEAPTMSi cause shear thinning in both polyethylene glycol and polypropylene glycol even at high shear rates. The reason for such high initial viscosities is the presence of big size flocs in the structure due to the higher interparticle interactions. Long chains in the structure of AEAPTMSi inhibit the interaction of surface amine groups with OH groups in the chain of polymeric fluids, thereby preventing the formation of the steric barrier which decreases the strength of interparticle interactions. Amino groups in the structure of AEAPTMSi perform a backbone structure; amino groups make hydrogen bonding with each other. Hydrogen bonding within the particles is leading to an increase in van der Waals interactions

which induce the agglomeration as well. The sharp decrease in the viscosity occurs due to the fact that big size flocs are broken by applied shear and the polymeric fluids entrapped by flocs are released, which leads to the decrease in the viscosity of the suspension. Further increase of shear forces (10 kPa) is not able to change the behavior of C3 and C7 since the higher interparticle interactions trigger gelation and forms strongly flocculated gels which are hard to deform. Thus, the applied shear force is not sufficient to initiate the transition from shear thinning to thickening regime.

Surface modification of fumed silica particles with quad silane results in shear thinning fluids for PEG whereas shear thickening fluid for PPG (Fig.4.27.a and b). C4 (QuadSi in PEG) and C8 (QuadSi in PPG) have high initial viscosities as C3 (AEAPTMSi in PEG) and C7 (AEAPTMSi in PPG) does due to existence of big size of flocs that are confirmed by cryo-TEM images in Fig.4.28.d and h. However, the initial viscosity of C4 is greater than of C8 (6866 Pa.s and 792.4 Pa.s respectively), which indicates the degree of flocculation in suspensions. High amount of flocculated structures are observed in C4 (QuadSi in PEG) as can be seen from the cryo-TEM image in Fig.4.28.d. Hence, it is expected that van der Waals interactions between particles in C4 will be higher since the long alkyl chain in the QuadSi will not allow for the formation of solvation layer on the surface of particles. Due to the length of the end group, particles preferentially form agglomerates. In C8 (QuadSi in PPG), agglomerated micro structures should also be expected due to the long chains of QuadSi. However, in C8, there exist steric forces to a certain degree in the system since the alkyl groups of PEG chains adheres to the surface of QuadSi through the alkyl groups in QuadSi. Thus, the degree of flocculation is expected to be lower in C8, leading to moderate size flocs. Upon the application of shear forces onto C4 (QuadSi in PPG) and C8 (QuadSi in PPG), van der Waals forces among particles are disrupted and in turn the entrapped liquid media within particles is released into the continuous media wherefore the viscosity decreases. The polymer chains will be aligned towards the direction of shear field, hence decrease the viscosity at low shear rates as well. However, C8 shows a shear thinning behavior over a wide range of shear rates followed by shear thickening behavior due to the interaction of C₁₄H₂₉ end of QuadSi with CH₃ groups in PPG chain.

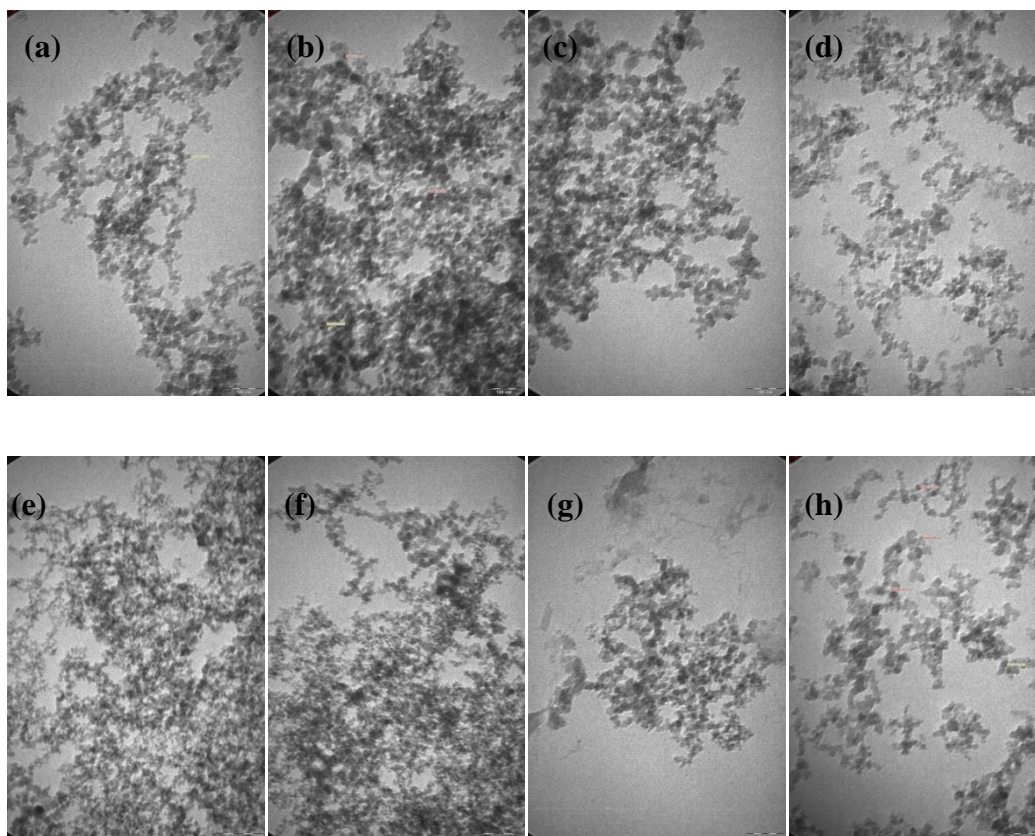


Fig. 4.28. cryo-TEM images (scale bar: 100 nm) for (a) C1 (b) C2 (c) C3 (d) C4 (e) C5 (f) C6 (g) C7 (h) C8

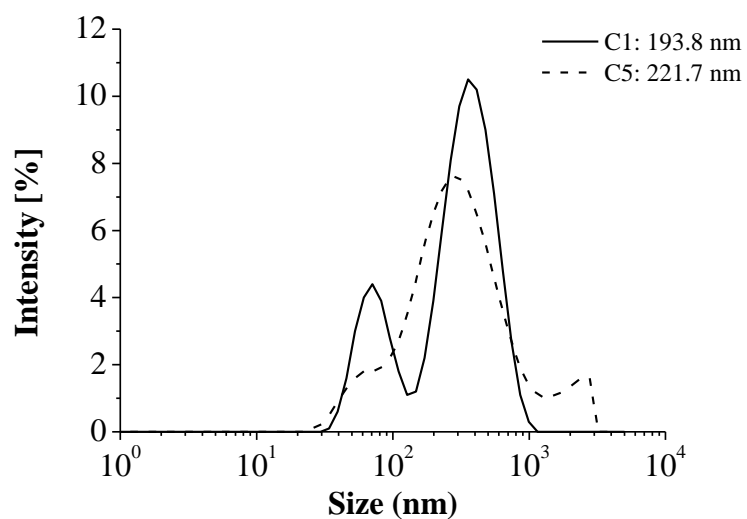


Fig. 4.29. DLS results of C1 (20 wt% HFSi in PEG) and C5 (20 wt% HFSi in PPG)

Colloidal interactions of modified silica particles in PEG and PPG were explained in terms of their viscosity profiles under steady shear. Flow behavior of the suspensions with the particle size of these colloids is summarized in Table.4. To conclude, HFSi and EPPTMSi particles exhibit shear thickening behavior in both PEG and PPG due to the hydrogen bonding of particles with polymeric media. Surface hydroxyls in HFSi and epoxide structure in EPPTMSi provide dispersion of the particles in PEG and PPG. Interparticle interaction performs steric barrier around the particles. However, amino groups in AEAPTMSi and QuadSi make hydrogen bonding within the particles which increase the van der Waals interaction in the suspensions. Van der Waals interaction results agglomeration and large size of flocs in the suspensions; exhibit shear thinning behavior. It can also be noted that, inconsistency of hydrodynamic radius and cryo-TEM images together with rheological analysis is related with the dilution of samples with ethanol for DLS and TEM analysis as well. Agglomeration is screened by dilution.

Table 4. Summary for flow behavior and hydrodynamic radius of suspensions C1-C8

Particle Type	Hydrodynamic Radius (HR) (nm)		Flow Behavior	
	PEG	PPG	PEG	PPG
HFSi	191.0	221.7	Shear Thickening(C1)	Shear Thickening (C5)
EPPTMSi	102.0	108.7	Shear Thickening (C2)	Shear Thickening (C6)
AEAPTMSi	83.6	101.8	Shear Thinning (C3)	Shear Thinning (C7)
QuadSi	94.1	97.3	Shear Thinning (C4)	Shear Thickening (C8)

4.3.2.2 Dynamic Rheological Analysis

Microstructure and its development in the suspensions are revealed by small amplitude oscillatory shear (SAOS) and large amplitude oscillatory shear (LAOS) experiments respectively. In SAOS, the structure is deformed slowly in the linear viscoelastic region (LVE) meaning that small perturbations are applied to the system to monitor the microstructural development under low shear stresses. Those experiments reveal the microstructure under stationary conditions. However, in LAOS experiments a large

amount of deformation is applied to monitor the microstructural development under shear conditions. Those experiments provide information about the non-linear response of the material. Steady shear experiment where gradual shear stress or rate is applied to the material, is also a non-linear experiment; but deformation is too fast so as the material has no time to respond to the environment. Steady shear experiments are not suitable to monitor the microstructural development under deformation [25].

Both small amplitude oscillatory shear (SAOS) and large amplitude oscillatory shear (LAOS) tests were conducted to reveal the microstructure under small and large deformations in suspensions C1-C8 and SAOS results for the suspensions are given in Fig.4.30. Suspensions both C1 (HFSi in PEG) and C5 (HFSi in PPG) (Fig.4.30.a and 4.30.e respectively) show liquid like behavior over the entire frequency range. Elastic and viscous modulus of C1 (HFSi in PEG) and C5 (HFSi in PPG) are frequency dependent and show a gradual increase under the entire range of deformation frequency. The viscous modulus of C1 in addition C5 are greater than of elastic modulus until the critical frequency at which G' and G'' begin to cross-over; transition from liquid to solid like behavior takes place. The transition from liquid-like to solid-like behavior also provides information about the initial microstructure of C1 and C5. When the complex viscosity of named suspensions is examined, it is seen that the viscosity decreases until a critical frequency and then begins to increase; transition from shear thinning to thickening takes place in C1 and C5. The complex viscosity of C1 and C5 show similar behavior with the viscosity profiles obtained in steady shear test given in Fig.4.27, but it should be noted that SAOS experiments are performed in LVE region and are non-destructive dynamic shear tests [25]. Thus, these suspensions are very sensitive to applied deformation; their response is quick to applied stress which is good in a sense for energy absorption applications.

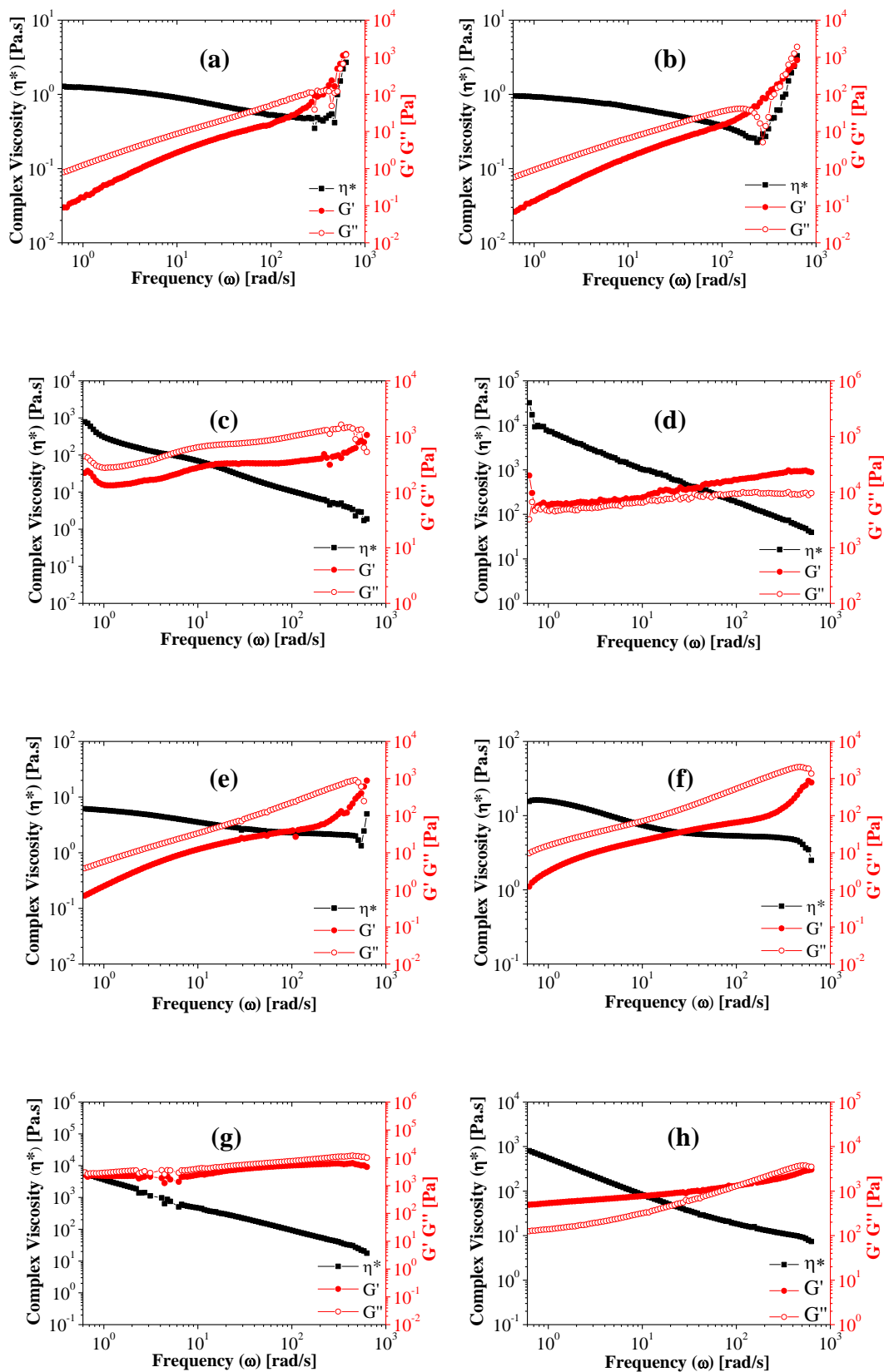


Fig. 4.30. Dynamic oscillatory frequency sweep in LVE region for suspensions;
(a) C1 **(b)** C2 **(c)** C3 **(d)** C4 **(e)** C5 **(f)** C6 **(g)** C7 **(h)** C8

Upon examining the behavior of C2 (Fig.4.30.b) and C6 (Fig.4.30.f) in SAOS experiments, they have a liquid-like structure initially; $G'' > G'$. Both elastic modulus and viscous modulus of C2 and C6 exhibit dependency on frequency. Frequency dependent elastic and viscous modulus behavior is an indicator for liquid-like structure initially as well. Shear thickening behavior is observed in C2 (EPPTMSi in PEG) at higher deformation frequencies where the G' starts to crossover G'' . But in C6 (EPPTMSi in PPG), gradual decrease of viscosity continues even at higher deformation frequencies (>100 rad/s). Higher degree of interparticle interaction in C6 (EPPTMSi in PEG) compared to C2 (EPPTMSi in PPG) can be contributed to shear thinning behavior. Although the complex viscosity of C6 (EPPTMSi in PPG) exhibit shear thinning behavior, increase in both G' and G'' is an indicator for shear thickening behavior upon the application of adequate deformation. C6 (EPPTMSi in PPG) exhibits shear thickening behavior in LAOS experiments shown in Fig.4.32.f. Elastic modulus (G') of C3 (AEAPTMSi in PEG) (fig.4.30.c) and C7 (AEAPTMSi in PPG) (Fig.4.30.g) does not exhibit dependency on frequency; they have a solid like microstructure and gelation, in a sense their internal structure contains large size of flocs. These results clarify the reason why these suspensions have a high initial viscosity. Same observation is shown in C4 (QuadSi in PEG) and C8 (QuadSi in PPG) in Fig.4.30.d and h respectively. Both C4 and C8 have solid-like structure initially; $G' > G''$. Linear behavior of G' over the entire range shows that material contains large size flocs that cannot be broken by small deformations. Gelation is also observed in these suspensions as in the case of C3 and C7. These findings as well as the high complex viscosity of C4 (QuadSi in PEG) and C8 (QuadSi in PPG) explain the high initial viscosity and shear thinning behavior in steady shear experiments.

To monitor the transition from linear to non-linear region at different deformation frequencies as well as the strain dependency of suspensions which provides information about the microstructure a strain sweep experiment was performed in a strain range (0.001-10 %) at constant frequencies (10 rad/s, 20 rad/s, 50 rad/s, and 100 rad/s) and results are shown in Fig.4.31.

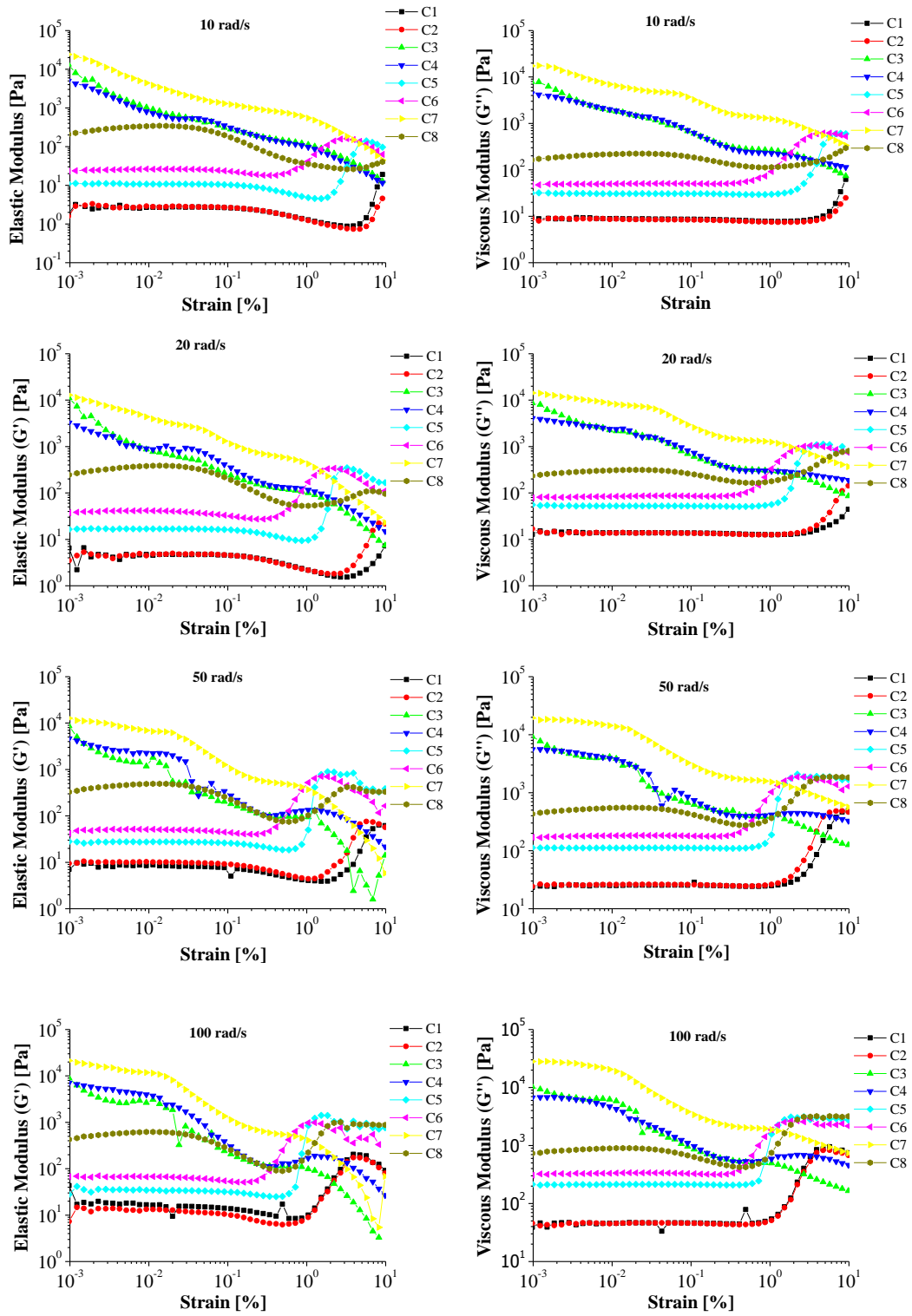


Fig. 4.31. Elastic and viscous modulus of colloids at varying frequencies; 10, 20, 50 and 100 rad/s.

In suspensions C1, C2, C5, C6 and C8, strain sweep results (Fig.4.31) indicate that critical strain shifts towards to smaller values as the frequencies increase. Nearly constant elastic and viscous module values are seen at lower strain values. Upon these suspensions reach the critical strain value under oscillatory deformations, their elastic and viscous modulus start to sharply increase. This increase becomes larger under deformations at higher frequencies (50 rad/s and 100 rad/s). This is evidence that they show shear thickening under large deformations. Another point is that, the increase in the elastic module of these suspensions after the critical strain value signs the strain hardening in these colloids. This is related with the breaking down of the microstructure. Agglomerated particles turn into small aggregates which cause an increase in viscous modulus. An associated increase in friction among these particles leads to an increase in viscous modulus due to higher energy dissipation. In C3, C4, and C7; both elastic and viscous moduli are strongly strain dependent; they tend to decrease with increasing strain value. However, they have a weak increase when these moduli reach a critical strain value; after that they tend to decrease again. This weak increase is seen at higher frequencies (100 rad/s). These findings indicate a gel-like structure at stationary conditions that differs from C1, C2, C5, C6 and C8 which are liquid like. C3, C4 and C7 are strongly flocculated structures at the beginning due to their strain dependency of their elastic moduli (G'). Larson et. al. shows that strongly flocculated gels have higher strain sensitivity compared to weak ones and they are more brittle [26]. This can also explain the reason why C3, C4 and C7 have high initial moduli. Recall that these suspensions show shear thinning behavior under steady shear.

For further analysis of colloidal suspensions at large amplitude oscillatory shear forces, frequency sweep tests were done under 1 strain which was selected from non-LVE region and results show that both G' and G'' for C1 and C2 have frequency dependency (Fig.4.32a-b). Greater G'' values at low frequencies (0.6 rad/s) implies that the energy dissipation by viscous forces are higher. They show liquid like behavior at low frequencies. Their complex viscosity starts to increase at a critical frequency value where G' starts to cross over G'' . Weak frequency dependence of G' , G'' for C3, C4, C7 compared to other suspensions is an indicator for the strong attractive inter particle interaction between disperse phase. Due to this strong interaction, more rigid and bigger size flocs are formed in the colloid. For that reason, bigger size flocs resist deformation under applied stress. It can be also noted that $G' > G''$, which suggest the formation of

gelation due to strong inter particle interaction. However at post frequency values (>100 rad/s), G' and G'' of C7 (AEAPTMSi in PPG) begin to increase and G' crossover G'' at a point where the complex viscosity has an increase. Although this suspension exhibits shear thinning behavior under steady shear, shear thickening behavior is observed at large deformation frequencies. As stated in the literature, all suspensions might exhibit shear thickening behavior under right conditions [2]. It is hard to monitor the rheological behavior of strongly flocculated gels by mechanical spectroscopy and more runs need to discard the scattered data [26]. C7 (AEAPTMSi in PPG) has noisy data points in its mechanical spectroscopy result in Fig.4.32.g. Therefore, this observation also supports the strongly agglomerated gel-like structure of C7 (AEAPTMSi in PPG) initially. The mechanical spectroscopy of C8 (QuadSi in PPG) in Fig.4.32.h shows that suspension exhibit shear thickening behavior after 100 rad/s. Recall that C8 exhibits shear thickening behavior with a high initial viscosity in the steady shear analysis shown in Fig.4.27.b. As stated before, while LAOS experiments mimics the rheological behavior under large deformations, SAOS experiments mimics the small deformation responses. Therefore, the result in Fig.4.32.h mimics the region of transition from shear thinning to shear thickening in the range of moderate shear rates to high shear rates in steady shear analysis in Fig.4.27. Low initial viscosity (40 Pa.s) in LAOS compared to the high initial viscosity (1 kPa.s) in SAOS might be attributed to the reason stated here. Rate of deformation affects the viscosity of soft gels in dynamic shear experiments.

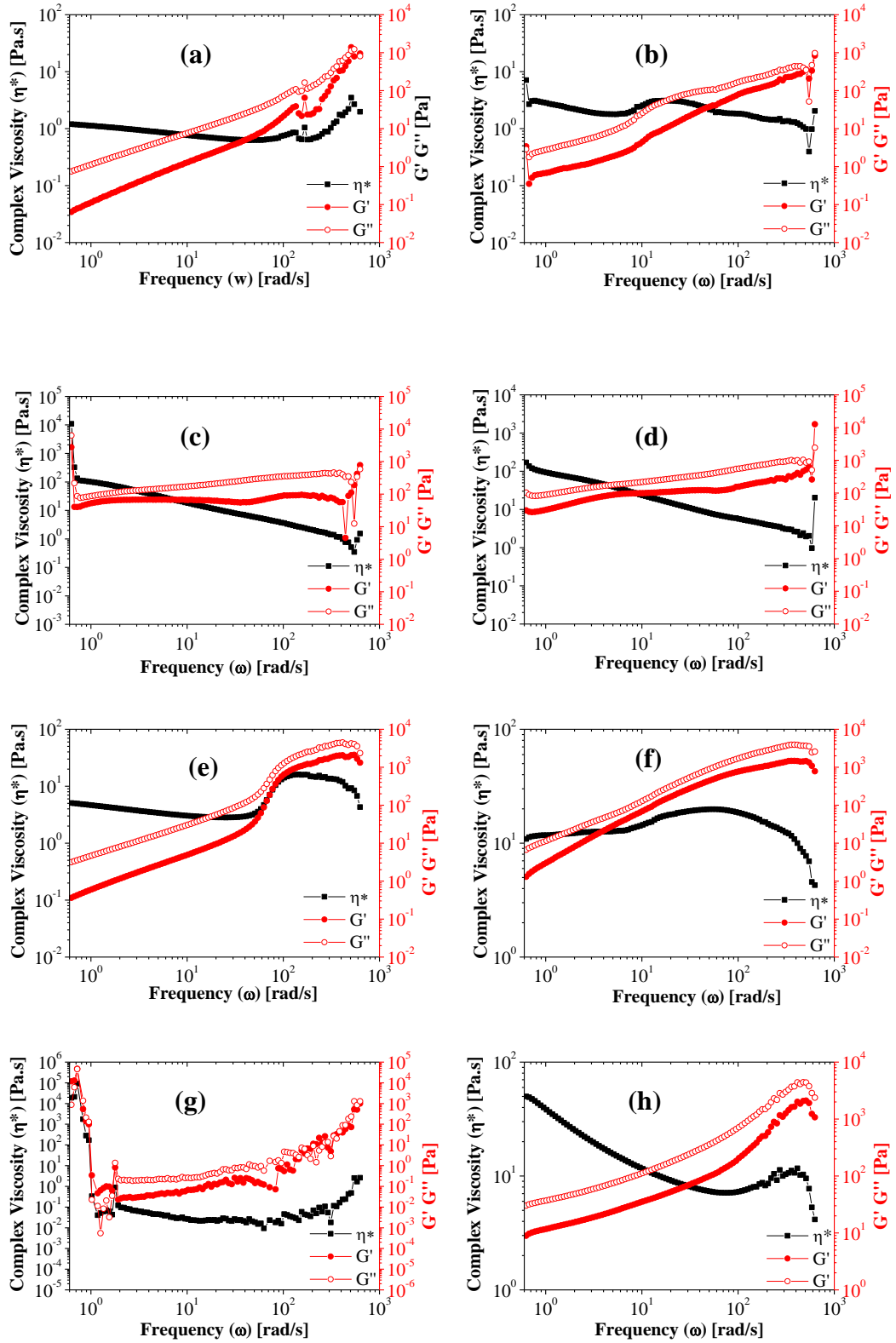


Fig. 4.32. Frequency sweep analysis in non-LVE region for (a) C1 (b) C2 (c) C3 (d) C4 (e) C5 (f) C6 (g) C7 (h) C8

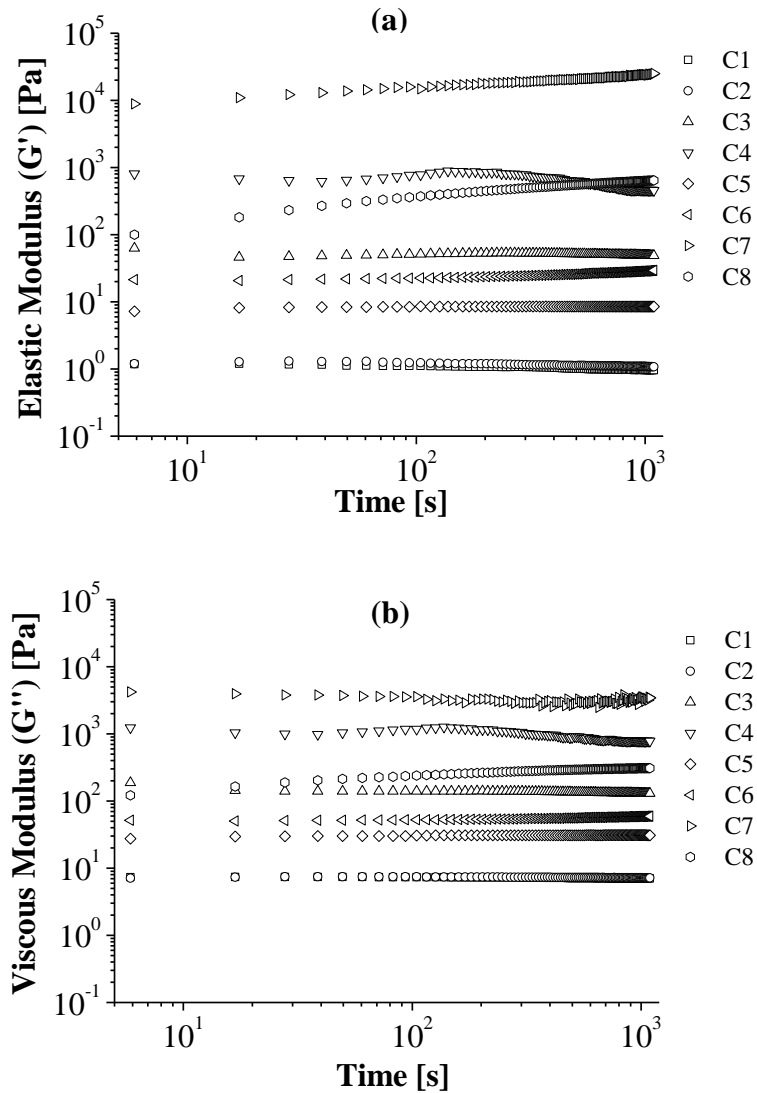


Fig. 4.33. Single frequency experiments results for samples C1-C8: **(a)** Elastic modulus **(b)** Viscous modulus

Fig.4.33 shows that elastic and viscous behavior of C1, C2, C5 and C6 do not change with time. This finding means that the time for reforming microstructure is long; the time given in the test was not sufficient to monitor it. Rapid increase in G' for C7 and C8 is attributed to the attractive van der Waals forces, hence are led to particle-particle interaction in these colloids. The viscous behavior of C7 does not change with time; however, the increase in the elastic behavior is an indicator for strong particle-particle linkage in the sample.

4.4 Temperature Effect

Temperature is an important parameter in the processing of polymeric fluids as well as suspensions. Temperature affects the movement of polymeric chains during flow; interactions between polymer chains get weaker and fewer; thus the viscosity of a polymer melt decreases with increasing temperature [54-56]. In addition to that, non-Newtonian suspensions show diverse trends in the variation of viscosity with temperature. The simplest case is that the change in viscosity with temperature for a suspension may simply reflect the change in the viscosity of the continuous phase. However, this trend is not observed with most non-Newtonian systems due to the change in the interparticle interaction with the increase in temperature [5]. In our study, the viscosity of continuous phases (PEG and PPG) decreases with increasing temperature; however, the viscosity of suspensions C1-C8 shows an increase as the temperature increases (Fig.4.30). The viscosity trends of continuous phase and the suspensions are not similar due to the change in interparticle interactions with temperature; thermal Brownian motion of silica particles in liquid medium and the hydrodynamic force inducing the dilatancy phenomenon increase as the temperature increases [57]. When a suspension shows flocculation above a critical temperature, the viscosity may show an initial decrease with increase of temperature, followed by an increase above the critical flocculation temperature [5]. This finding might explain the viscosity behavior in the given suspensions as well as the microstructural development under varying temperature given in Fig.4.30 and 4.31 respectively. Formations of flocs in the system result in high viscosity together with gelation as stated in previous sections.

It should be noted that shear thinning behavior is observed in certain colloids under steady and dynamic shear stresses (C4). Although C4 is shear thinning fluid; it exhibits shear thickening behavior with increasing temperature due to sol gel transition (Fig.4.31.b). Transition from sol to gel takes place at a critical temperature where G' (elastic modulus) cross-over G'' (viscous modulus). At that point; there is an abrupt increase in viscosity. Gel like response sustains for an entire range; because applied shear stress is not sufficient to break down the structure [55]. To check the reversibility of sol-gel transition the same samples are subjected to 125-25°C temperature cooling

(with a cooling rate of 5°C/min). Results (data not given here) showed that sol-gel transition is reversible but not in a perfect manner.

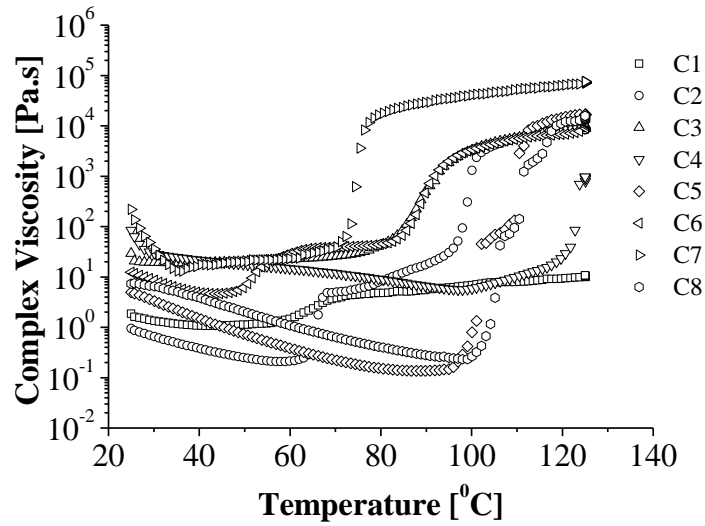


Fig. 4.34. Viscosity profile of colloidal suspensions with temperature change (25-125°C)

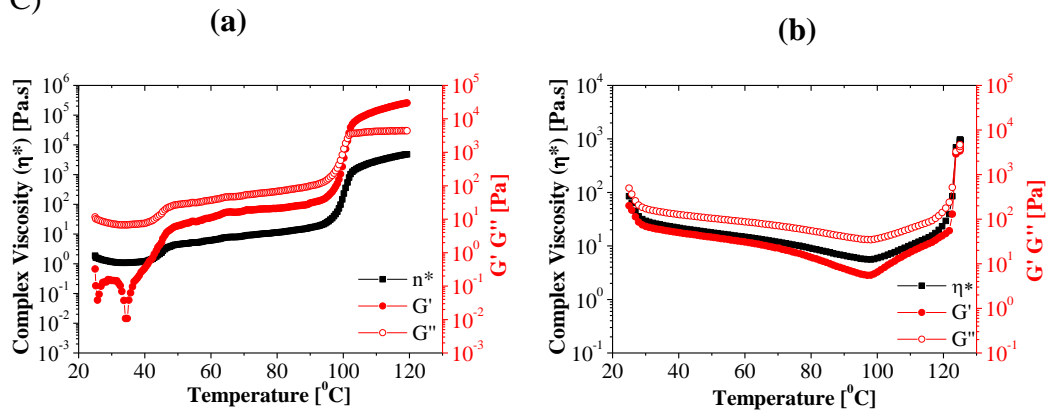


Fig. 4.35. Dynamic rheological response of (a) C1 and (b) C3 within the temperature range of 25-125°C

CHAPTER V

5 CONCLUSION AND FUTURE WORK

Parameters effecting on the rheology of polymeric colloids and suspensions have been investigated in this study. Those suspensions were composed of anisotropic, agglomerated particles with low volume fraction. There has not been detailed research in terms of the rheological response (shear thickening mechanism) of those suspensions in the literature. In this regard the conclusion of this study can be summarized as follows:

Electrical resistance measurements were done simultaneously with steady shear rheological analysis to understand the mechanism behind shear thickening and shear thinning behavior. Electrical resistance response of conductive particles (CNT and graphene) dispersed in a non-conductive medium (PEG) were measured under shear forces. In shear thinning region, there is a rise in resistance due to liberate of polymeric media after break down of agglomerates. However, in shear thickening region, a sudden drop in electrical resistance was measured due to the fact that effective volume fraction of conductive particles increases upon the breakage of agglomerates and they begin to percolate and perform a network structure.

In order to investigate the particle morphology, structure and size effects on rheology of polymeric dispersions, halloysite, clay, organoclay, CNT, graphene particles were dispersed in polyethylene glycol. Results show that particle morphology and size have significant effect on the rheology polymeric dispersions. Suspensions with organoclay particles exhibit shear thickening behavior under large steady shear forces and deformation frequencies due to the fact that layered silicates behave as fractals and anisotropic behavior of these layers increase the viscosity. Shear thinning behavior was observed in suspensions with CNT particles and a weak dispersion of CNT in polyethylene glycol at high particle loadings (5 wt% and 10 wt %) was confirmed by the TEM images. A large amount of agglomeration in CNT was observed due to the high interparticle interactions which cannot be weakened by steric forces. Steady and dynamical experiments show that applied shear forces are not sufficient to break down

the agglomerates into aggregates to obtain high surface area in particles since the high surface area tends to increase the viscosity at critical shear rate at which transition from shear thinning to shear thickening takes place. Suspensions with graphene particles exhibit shear thickening behavior at higher shear rates (17k s^{-1}) and great amount of shear forces (5k Pa) are needed to be applied to the suspension since big size agglomerates are formed in the suspension due to the depletion forces between particles. To conclude, anisotropy affects the rheological behavior of suspensions; it increases viscosity due to the low amount of effective volume fraction. However, observance of shear thickening behavior in the suspensions containing anisotropic particles takes place at high shear rates regarding to their large particle size and their agglomeration due to attractive interparticle interactions.

Fumed silica particles were modified with epoxy, amine and quaternized ammonium end silane agents to investigate the effect of the surface characteristics of the particle on the deformation and flow behavior of polymeric dispersions. Particles with epoxide functional groups shows shear thickening behavior in both PEG and PPG with better dispersion compared with fumed silica. The reason for the shear thickening behavior is the finely dispersed particles in polymeric fluid due to the hydrogen bonding through the epoxide group in EPPTMSi and hydroxyl groups in the named polymeric fluid, since friction between finely dispersed particles will be higher. However particles with amine end groups show shear thinning due to the fact that amine groups in AEAPTMSi cause the formation of large flocs because of high interparticle interactions between AEAPTMSi. Colloidal suspensions composed of QuadSi particles either in PEG and PPG shows large size flocs due to the long chain of QuadSi. Suspension in PEG show shear thickening behavior over wide shear rate range whereas in PPG shows shear thinning behavior followed by shear thickening due to the interaction alkyl groups in QuadSi through CH_3 in PPG. Under high deformation frequencies and stress, all suspensions except QuadSi in PEG exhibit shear thickening behavior. Changing surface properties of nanoparticles provide diverse rheological behavior for polymeric dispersions. This finding is useful especially in the processing of nano particle filled polymeric fluids, since “tunable nano materials” can be produced upon application.

Viscosity change in colloids with respect to varying temperature was also investigated. It is surprisingly observed that; there is an abrupt increase in viscosity with increasing

temperature; the thermal Brownian motion of silica particles in liquid medium as well as the hydrodynamic force inducing the dilatancy phenomenon increases as the temperature increases. Sol-gel transition was observed in colloidal from dynamic rheological analyses after a critical temperature. This transition point differs in all colloidal suspensions; the degree of flocculation in the suspension shifts the transition point from high to low temperatures.

It can be concluded that, as stated in many published researches about shear thickening behavior, that all suspensions might exhibit shear thickening behavior under right the conditions. Those conditions are defined as shear stress, volume fraction of particles in the suspension, particle size and anisotropy as well as colloidal interactions such as short range attractive forces, repulsive steric forces, and so on; our experimental finding in this study confirm this statement.

Investigation of the rheology of surface modified silica particles with diverse polar end groups upon which literature exist to date is one of the main research topics in this study. Findings of this unique research enable to design tunable nanomaterials upon application as stated before in that section.

As a future work, the first ballistic performance of silica suspensions might be examined. There is an ongoing project with Kuleli Military High School about the application of shear thickening fluid as a liquid armor. The second, silane coupling agents with non-polar end groups such as hexamethyldisilazane might be used to modify the surface of fumed silica particles with non-polar groups so as to understand the effect of hydrophobic interactions on the rheology. Lastly, ionic systems might also be used so as to make further analysis of shear thickening behavior in another aspect.

REFERENCES

1. Hoffman, R.L., *Discontinuous and Dilatant Viscosity Behavior in Concentrated Suspensions. I. Observation of a Flow Instability*. Journal of Rheology, 1972. **16**(1): p. 155.
2. Barnes, H.A., *Shear thickening (Dilatancy) in suspensions of nonaggregating solid particles dispersed in Newtonian fluids*. Journal of Rheology, 1989. **33**(2).
3. Bender, J., *Reversible shear thickening in monodisperse and bidisperse colloidal dispersions*. Journal of Rheology, 1996. **40**(5): p. 899.
4. Genovese, D.B., *Shear rheology of hard-sphere, dispersed, and aggregated suspensions, and filler-matrix composites*. Adv Colloid Interface Sci, 2012. **171-172**: p. 1-16.
5. F., T.T., *Rheology of Dispersions in Principles and Applications* 2010, Wiley-VCH: Singapore.
6. Mewis, J.a.W., N.J., *Colloidal Suspension Rheology*. 2012, New York, USA: Cambridge University Press.
7. D.J., S., *Introduction to Colloid and Surface Chemistry*. 4th Edition ed. 1992, UK: Butterworth-Heinemann.
8. Chhabra R.P., a.R.J.F., *Non-Newtonian Flow in the Process Industries*. 1999, India: Butterworth-Heinemann.
9. Croce, F., Persi, L. Ronci, F. Scrosati, B., *Nanocomposites polymer electrolytes and their impact on the lithium battery technology*. Solid State Ionics, 2000. **135**: p. 45-52.
10. Croce, F., et al., *Nanocomposite polymer electrolytes for lithium batteries*. Nature, 1998. **394**(6692): p. 456-458.
11. Eesa, M. and Barigou, M., *CFD investigation of the pipe transport of coarse solids in laminar power law fluids*. Chemical Engineering Science, 2009. **64**(2): p. 322-333.
12. Zhang, X.Z., Li, W. H., Gong X. L., *The rheology of shear thickening fluid (STF) and the dynamic performance of STF-filled damper*. Smart. Mater. Struct., 2008. **17**: p. 7.
13. Hassan, T.A., Rangari, V. J., Jeelani, S., *Synthesis, processing and characterization of shear thickening fluid (STF) impregnated fabric composites*. Materials Science and Engineering A, 2010. **527**: p. 2892-2899.
14. Fischer, C., Braun, S. A., Bourban, P-E., Michaud, V., et al., *Dynamic properties of sandwich structures with integrated shear thickening fluids*. Smart. Mater. Struct., 2006. **15**: p. 1467-1465.
15. Decker, M.J., et. al, *Stab resistance of shear thickening fluid (STF)-treated fabrics*. Composites Science and Technology, 2007. **67**: p. 565-578.
16. Sirivastava, A., Majumdar, A., Butola, B. S., *Improving the impact resistance performance of Kevlar fabrics using silica based STF*. Materials Science and Engineering A, 2011. **529**: p. 224-229.

17. Lomakin, E.V., Mossakovsky, P.A., Bragov, A.V., Lomunov, A.K., Konstantinov, A. Yu., Kolotnikov, M.E., Antonov, F.K, Vaksthein, M.S., *Investigation of impact resistance of multilayered composite barrier with shear thickening fluid*. Arch. Appl. Mech., 2011. **81**: p. 2007-2020.
18. Park, J.H., Yoon, B., Paik, J.G., Kang, T.J., *Ballistic performance of p-aramid fabrics with shear thickening fluid; Part I-Effect of laminating sequence*. Textile Research Journal, 2012. **82**(6): p. 527-541.
19. Hoffman, R.L., *Explanations for the cause of shear thickening in concentrated colloidal suspensions*. Journal of Rheology, 1998. **42**(1): p. 111.
20. Maranzano, B.J. and Wagner, N.J., *The effects of interparticle interactions and particle size on reversible shear thickening: Hard-sphere colloidal dispersions*. Journal of Rheology, 2001. **45**(5): p. 1205.
21. Laun, H.M.e.a., *Rheological and small angle neutron scattering investigation of shear-induced particle structures of concentrated polymer dispersions submitted to plane Poiseuille and Couette flow*. Journal of Rheology, 1992. **36**(4): p. 743.
22. Negi, A.S. and Osuji, C.O., *New insights on fumed colloidal rheology—shear thickening and vorticity-aligned structures in flocculating dispersions*. Rheologica Acta, 2008. **48**(8): p. 871-881.
23. Osuji, C.O., Kim, C., and Weitz, D.A., *Shear thickening and scaling of the elastic modulus in a fractal colloidal system with attractive interactions*. Physical Review E, 2008. **77**(6).
24. Goodwin J.W., a.H.R.W., *Rheology for Chemists: An Introduction*. 2nd Edition ed. 2008: RSC Publishing.
25. Deshpande A., K.J.M., Kumar P.B., , *Rheology of Complex Fluids*. 2010: Springer. 270.
26. R.G., L., *The Structure and Rheology of Complex Fluids*. 1999, NewYork: Oxford University Press.
27. Demir, M.M. and Wegner, G., *Challenges in the Preparation of Optical Polymer Composites With Nanosized Pigment Particles: A Review on Recent Efforts*. Macromolecular Materials and Engineering, 2012. **297**(9): p. 838-863.
28. Ettliger, M., Ladwig, T., Weise A., *Surface modified fumed silicas for modern coatings*. Progress in Organic Coatings, 2000. **40**: p. 31-34.
29. Zou, H., Wu, S., and Shen, J., *Polymer/Silica Nanocomposites: Preparation, Characterization, Properties, and Applications*. ACS Chem. Rev., 2008. **108**: p. 3893-3957.
30. Mahfuz, H., et al., *Enhanced stab resistance of armor composites with functionalized silica nanoparticles*. Journal of Applied Physics, 2009. **105**(6).
31. Galindo-Rosales, F.J., Rubio-Hernández, F.J., and Velázquez-Navarro, J.F., *Shear-thickening behavior of Aerosil® R816 nanoparticles suspensions in polar organic liquids*. Rheologica Acta, 2009. **48**(6): p. 699-708.
32. Isci, S., et al., *Influence of Clay Surface Modification on Morphology and Rheology of Polyethylene Glycol/Montmorillonite Nanocomposites*. Journal of Composite Materials, 2007. **41**(12): p. 1521-1533.

33. Kumar, S., Tiwari, S., Nagaralli, B., Steinberger, H., *Facile synthesis of functionalized nano silica: Effect of microstructure on the physical properties of LSR*. Rubber World, 2009.
34. Luo, Z., et al., *One-step synthesis of functional silica nanoparticles for reinforcement of polyurethane coatings*. Powder Technology, 2012. **218**: p. 23-30.
35. Yu, K., et al., *Shear-thickening behavior of modified silica nanoparticles in polyethylene glycol*. Journal of Nanoparticle Research, 2012. **14**(3).
36. Ragvahan, S.R., Khan, S. A. , *Shear Thickening Response of Fumed Silica Suspensions Under Steady and Oscillatory Shear*. Journal of Colloid and Interface Science, 1997. **185**: p. 57-67.
37. Ozel, B., *Polymer particle interactions in nanocolloids*, in Graduate School of Engineering and Natural Sciences 2011, Sabancı University: Istanbul.
38. Saner, B., Okyay, F., and Yurum, Y., *Utilization of multiple graphene layers in fuel cells. 1. An improved technique for the exfoliation of graphene-based nanosheets from graphite*. Fuel, 2010. **89**: p. 1903-1910.
39. Yearsley, K.M., et al., *The rheology of multiwalled carbon nanotube and carbon black suspensions*. Journal of Rheology, 2012. **56**(6): p. 1465.
40. Endo, M., Ijima, S., and Dresselhaus, M.S., *Carbon Nanotubes*, 1996, Pergamon.
41. Butler S. Z., e.a., *Progress, Challenges, and Opportunities in Two-Dimensional Materials Beyond Graphene*. ACS NANO, 2013. **7**(4): p. 2898-2926.
42. Guimont, A., et al., *Viscoelasticity of Graphite Oxide-Based Suspensions in PDMS*. Macromolecules, 2011. **44**(10): p. 3893-3900.
43. Alexandre M., D.P., *Polymer-layered silicate nanocomposites: preparation, properties and uses of a new class of materials*. Materials Science and Engineering, 2000. **28**: p. 1-63.
44. Brader, J.M., *Nonlinear rheology of colloidal dispersions*. J Phys Condens Matter, 2010. **22**(36): p. 363101.
45. Jenny Hilding, E.A.G., Z. George Zhang, and Fran Lockwood, *Dispersion of Carbon Nanotubes in Liquids*. Journal of Dispersion Science and Technology, 2003. **24**(1).
46. Lee, Y.S., and Wagner, N. J., *Dynamic properties of shear thickening colloidal suspensions*. Rheologica Acta, 2003. **42**: p. 199-208.
47. Cassagnau, P., *Linear viscoelasticity and dynamics of suspensions and molten polymers filled with nanoparticles of different aspect ratios*. Polymer, 2013. **54**(18): p. 4762-4775.
48. Raos G., M.M., and Elli S., *Computational Experiments on Filled Rubber Viscoelasticity: What is the Role of Particle-Particle Interactions?* Macromolecules, 2006. **39**(19): p. 6744-6751.
49. Jung, Y., et al., *Rheological behavior of clay-nanoparticle hybrid-added bentonite suspensions: specific role of hybrid additives on the gelation of clay-based fluids*. ACS Appl Mater Interfaces, 2011. **3**(9): p. 3515-22.

50. Majumdar S., K.R., Sood A. K., *Discontinuous shear thickening in confined dilute suspensions*. PNAS, 2011. **108**(22): p. 8996-9001.
51. Ma, A.W.K., Mackley, M.R., and Chinesta, F., *The microstructure and rheology of carbon nanotube suspensions*. International Journal of Material Forming, 2008. **1**(2): p. 75-81.
52. Yokozeki, T., et al., *Investigation of shear thinning behavior and microstructures of MWCNT/epoxy and CNF/epoxy suspensions under steady shear conditions*. European Polymer Journal, 2012. **48**(6): p. 1042-1049.
53. Raghavan S.R., W.H.J., and Khan S., *Rheology of Silica Dispersions in Organic Liquids: New evidence for solvation forces dictated by hydrogen bonding*. Langmuir, 2000. **16**(21): p. 7920-7930.
54. Peacock A. J., C.A., *Polymer Chemistry: Properties and Applications*. 2006, Munich: Hanser.
55. Park, J.-H., et al., *Rheological behavior of hydrophilic silica dispersion in polyethylene glycol*. Journal of Applied Polymer Science, 2007. **103**(4): p. 2481-2486.
56. D., H.C., *Rheology and Processing of Polymeric Materials*, in *Volume 1, Polymer Rheology* 2007, Oxford University Press.
57. Boersma W.H., L.J., and Stein H.N., *Shear Thickening (Dilatancy) in Concentrated Suspensions*. AIChE J, 1990. **36**(3).